HAL
open science

Aluminium in an ocean general circulation model compared with the West Atlantic Geotraces cruises

Marco van Hulten, Andreas Sterl, Alessandro Tagliabue, Jean-Claude Dutay, Marion Gehlen, Hein J. W. de Baar, Rob Middag

To cite this version:

Marco van Hulten, Andreas Sterl, Alessandro Tagliabue, Jean-Claude Dutay, Marion Gehlen, et al.. Aluminium in an ocean general circulation model compared with the West Atlantic Geotraces cruises. Journal of Marine Systems, 2013, 126, pp.3-23. 10.1016/j.jmarsys.2012.05.005 . cea-00917283

HAL Id: cea-00917283

https://cea.hal.science/cea-00917283v1

Submitted on 24 Jun 2021

HAL is a multi-disciplinary open access archive for the deposit and dissemination of scientific research documents, whether they are published or not. The documents may come from teaching and research institutions in France or abroad, or from public or private research centers.

L'archive ouverte pluridisciplinaire **HAL**, est destinée au dépôt et à la diffusion de documents scientifiques de niveau recherche, publiés ou non, émanant des établissements d'enseignement et de recherche français ou étrangers, des laboratoires publics ou privés.

Journal of Marine Systems 126 (2013) 3–23

Contents lists available at ScienceDirect

Journal of Marine Systems

journal homepage: www.elsevier.com/locate/jmarsys

Aluminium in an ocean general circulation model compared with the West Atlantic Geotraces cruises☆

M.M.P. van Hulten [a,*], A. Sterl [a], A. Tagliabue [b,c,g], J.-C. Dutay [c], M. Gehlen [c], H.J.W. de Baar [d,e], R. Middag [e,f]

[a] Royal Netherlands Meteorological Institute (KNMI), De Bilt, The Netherlands
[b] University of Cape Town (UCT), Cape Town, South Africa
[c] Laboratoire des Sciences du Climat et de l'Environnement (LSCE), Gif sur Yvette, France
[d] University of Groningen (RUG), Groningen, The Netherlands
[e] Royal Netherlands Institute for Sea Research (NIOZ), Den Burg, The Netherlands
[f] University of California Santa Cruz (UCSC), Santa Cruz, CA, USA
[g] Southern Ocean Carbon and Climate Observatory (SOCCO), CSIR, Stellenbosch, South Africa

ARTICLE INFO

Article history:
Received 30 September 2011
Received in revised form 11 May 2012
Accepted 16 May 2012
Available online 25 May 2012

Keywords:
Aluminium
Dust deposition
Modelling
PISCES
Scavenging
West Atlantic Ocean
GEOTRACES

ABSTRACT

A model of aluminium has been developed and implemented in an Ocean General Circulation Model (NEMO-PISCES). In the model, aluminium enters the ocean by means of dust deposition. The internal oceanic processes are described by advection, mixing and reversible scavenging. The model has been evaluated against a number of selected high-quality datasets covering much of the world ocean, especially those from the West Atlantic Geotraces cruises of 2010 and 2011. Generally, the model results are in fair agreement with the observations. However, the model does not describe well the vertical distribution of dissolved Al in the North Atlantic Ocean. The model may require changes in the physical forcing and the vertical dependence of the sinking velocity of biogenic silica to account for other discrepancies. To explore the model behaviour, sensitivity experiments have been performed, in which we changed the key parameters of the scavenging process as well as the input of aluminium into the ocean. This resulted in a better understanding of aluminium in the ocean, and it is now clear which parameter has what effect on the dissolved aluminium distribution and which processes might be missing in the model, among which boundary scavenging and biological incorporation of aluminium into diatoms.

© 2012 Elsevier B.V. Open access under CC BY-NC-ND license.

1. Introduction

The distribution and cycling of aluminium (Al) in the ocean has received attention for a variety of reasons. Firstly, if the Al cycle is understood well, aluminium surface concentrations can be used to constrain atmospheric dust deposition fields (Gehlen et al., 2003; Han, 2010; Han et al., 2008; Measures et al., 2005, 2010), which are used to predict aeolian iron addition to the euphotic zone. This is important, since iron is an essential trace-nutrient for phytoplankton; thus its availability has a direct consequence on primary production and air–sea CO_2 exchange (Boyd et al., 2007; de Baar et al., 2005; Martin, 1990).

Secondly, there is evidence that Al inhibits the solubility of sedimentary biogenic silica (Dixit et al., 2001; Emerson and Hedges, 2006; Lewin, 1961; Sarmiento and Gruber, 2006; van Bennekom et al., 1991). If less biogenic silica gets dissolved from sediments, eventually there will be less silicic acid available in the euphotic zone, which will reduce diatom production as silicon is an essential major nutrient for diatoms. Modified diatom productivity will impact ocean food webs and the export of organic carbon to the ocean's interior. For advancement in both of these fields of interest a good understanding of the Al cycle is pertinent.

Currently it is assumed that the major source of Al to the ocean is via dust deposition (e.g. Kramer et al., 2004; Maring and Duce, 1987; Measures et al., 2005; Orians and Bruland, 1986). When dust enters the ocean, a part of its aluminium content (1–15%) dissolves in the uppermost layer and is quickly distributed over the mixed layer by turbulent mixing. Most dust remains in the particulate phase and sinks to the bottom of the ocean, while a small fraction might dissolve in the water column. The dust that does not dissolve at all is buried in the sediment (Gehlen et al., 2003; Sarmiento and Gruber, 2006).

Arguments that dissolution occurs primarily in the upper layer of the ocean come from shipboard experiments and atmospheric moisture considerations. Maring and Duce (1987) and Measures et al. (2010) showed that within a day after deposition, most of the dissolvable Al will be dissolved. Assuming a sinking speed of dust of 30 m/day, most Al would then dissolve in the upper 30 m of the ocean. This depth is shallower than the mixed layer depth, which means that there is little dissolution below the mixed layer.

Even though some earlier studies showed that most deposition is dry (Jickells, 1995; Jickells et al., 1994), more recent work shows that dust deposition is mostly wet (Guerzoni et al., 1997; Vink and

☆ http://arxiv.org/abs/1202.4679.

* Corresponding author. Tel.: +31 30 2206 707.
E-mail address: hulten@knmi.nl (M.M.P. van Hulten).

0924-7963 © 2012 Elsevier B.V. Open access under CC BY-NC-ND license.
doi:10.1016/j.jmarsys.2012.05.005

Measures, 2001). It has been argued that most dust passes through low pH environments in the atmosphere, which means that for wet deposition Al is already dissolved when it enters the ocean surface. Since the wetly deposited Al is most important, dissolution in the surface ocean is most relevant (as a lower bound, since dry deposition results in both surface and water column dissolution). Furthermore, based on the same low pH argument, dissolvable Al from dry deposition is likely to instantaneously dissolve in the surface ocean (Measures et al., 2010, and references herein), making the relative amount of surface dissolution even higher compared to water column dissolution.

Fluvial input can be thought to be important as well, since rivers carry large concentrations of Al, but in estuaries and coastal regions this Al is removed by scavenging of Al onto particles (Brown et al., 2010; Mackin, 1986; Mackin and Aller, 1986; Orians and Bruland, 1986). There are also indications for Al input as a consequence of sediment remobilisation, as in the Arctic Ocean (Middag et al., 2009) and North Atlantic Ocean (Moran and Moore, 1991). However, the importance of sedimentary sources can vary by basin (e.g. in the Southern Ocean these are small as shown by Moran et al. (1992) and Middag et al. (2011)). Finally, hydrothermal vents are thought to only play a minor role (e.g. Hydes et al., 1986; Middag, 2010). In summary, the dominant external source of aluminium in the ocean is atmospheric dust deposition.

Dissolved aluminium (Al_{diss}) is removed mainly by particle scavenging (Bruland and Lohan, 2006; Moran and Moore, 1989; Orians and Bruland, 1986; Stoffyn and Mackenzie, 1982). This is the combination of adsorption onto a solid surface, followed by sinking due to insufficient buoyancy of the particulates in the seawater (Bacon and Anderson, 1982; Bruland and Lohan, 2006; Goldberg, 1954). Typically, scavenging is deemed to be reversible, which means that during sinking release of the adsorbed, or particulate, aluminium (Al_{ads}) may occur. This happens both directly (by desorption) and indirectly (by dissolution of the biogenic carrier particles). As a consequence, Al_{diss} concentrations increase with depth (Anderson, 2006; Bacon and Anderson, 1982). In this way Al_{diss} is distributed over depth more efficiently than due to mixing and water mass transport. Aluminium is scavenged relatively efficiently and therefore has a relatively short residence time in the ocean (100–200 years) (Orians and Bruland, 1985).

Except for scavenging, there are strong suggestions from observations in certain regions that Al is biologically incorporated into the siliceous cell walls of diatoms (Gehlen et al., 2002; MacKenzie et al., 1978; Moran and Moore, 1988; Stoffyn, 1979). It seems that Al does not play an essential role for the diatoms, but it can be incorporated functioning as a replacement for silicon (Si), since it is similar in size. Therefore it is likely that the incorporation ratio Al:Si is close to that of the surrounding waters. These regions include the Arctic Ocean (Middag et al., 2009) and the Mediterranean Sea (Chou and Wollast, 1997; Hydes et al., 1988; MacKenzie et al., 1978). Given the ratio Al:Si of incorporation into the diatom in the photic zone, after remineralisation anywhere in the water column, the same dissolved Al:Si will be present, as long as this is the only source of Al and Si. When the dissolved Al and Si is then advected into the Atlantic Ocean by the North Atlantic Deep Water (NADW), this signal slowly disappears because of other sources of Al among which dust deposition and possibly sediment resuspension (Middag et al., 2011) and a source of Si from Antarctic Bottom Water.

Recent years have seen the development of models of the marine biogeochemical cycle of Al. Gehlen et al. (2003) implemented a basic scavenging model, while Han et al. (2008) also included a biological aluminium incorporation module.

Gehlen et al., (2003) had the objective of testing the sensitivity of modelled Al fields to dust input and thus to evaluate the possibility for constraining dust deposition via Al_{diss}. To this purpose they embedded an Al cycle in the HAMOCC2 biogeochemical model. The model consists of an equilibrium relation between, on the one hand, Al_{ads} and, on the other hand, Al_{diss}. In chemical equilibrium Al_{ads} is proportional to the biogenic silica ($bSiO_2$) concentration. In their work, as well as this paper, the term biogenic silica or $bSiO_2$ refers to the detrital fractions which is fuelled by diatoms and other silicifying phytoplankton, which have no stable organic matter coating and sink. When $bSiO_2$ sinks to the seafloor (together with adsorbed Al), it is buried. The resulting concentration of modelled Al_{diss} was of the same order as the then published observations, but it suggested a significant overestimation of Saharan dust input (Gehlen et al., 2003) when the dust deposition field of Mahowald et al. (1999) was used.

The main goal of Han et al. (2008) was to better constrain the dust deposition field. For this purpose they used the Biogeochemical Elemental Cycling (BEC) model improved by Moore et al. (2008) as a starting point. They used all dissolved Al datasets used by Gehlen et al. (2003) and added more datasets. Except for scavenging Han et al. (2008) added a biological Al uptake module where the Al:Si uptake ratio is a function of the ambient Al and Si concentrations (Han et al., 2008). The surface residence time of Al for both modelling studies varies strongly between different locations (from less than 1 year to almost 80 years), consistent with other estimates (Orians and Bruland, 1986; Maring and Duce, 1987; Moran et al., 1992).

Overall, there are a number of questions regarding the oceanic Al cycle that remain to be fully addressed. These touch on issues of ocean circulation, the specific sources and sinks of Al in different parts of the world ocean and what processes are needed to accurately simulate the oceanic distribution of Al.

Firstly, there is the question of the meridional (north to south) distribution of Al through the Atlantic Ocean. In the North Atlantic Ocean and northern seas, water sinks and forms NADW, which is then transported southward (e.g., Gary et al., 2011; Lozier, 2010). In the deep Atlantic Ocean dissolved silicon (Si) concentration increases from north to south (Ragueneau et al., 2000; Sarmiento and Gruber, 2006), while the concentration of Al_{diss} stays relatively constant until about 20°S and then decreases (Middag et al., in preparation; see also Section 4.5). Thus it has a generally opposite behaviour compared to Si. Since there are strong suggestions that the processes controlling the distribution of Si and Al are linked, the question is raised how this negative correlation is possible.

Secondly, there is the question about the observed profiles of Al_{diss} at different locations in the ocean. Generally, profiles of Al_{diss} have a reversible-scavenging profile (increasing with depth) and often with a minimum near 1 km depth and a maximum at the surface because of dust deposition. However, observations in the Mediterranean Sea (Chou and Wollast, 1997; Hydes et al., 1988) and IPY-Geotraces-NL observations in the eastern Arctic (Middag et al., 2009) show that there is a strong positive relation between aluminium and silicon. This supports the hypothesis of biological incorporation of aluminium into the cell wall of diatoms.

These issues can be analysed further by the use of numerical models. Since there is a strong spatial variation in aluminium concentration (and its relation to silicon), an ocean general circulation model should be used to simulate the distribution of Al_{diss}. Potentially crucial parameters and sources can be modified in the model to test its sensitivity to these changes. In this way a better understanding of the aluminium cycle can be reached.

In this paper the observed distribution of Al is modelled and the processes driving it are examined. Based on new observations and previous work on aluminium modelling (Gehlen et al., 2003; Han et al., 2008) a model of aluminium based on dust deposition and scavenging by biogenic silica is formulated. This model and the configuration of the simulations will be set out in the following section. Then the observations which are used to check and improve the model will be discussed. The results of the several experiments follow in Section 3, as well as a comparison with the observations. The discussion in Section 4 comprises of a comparison between our model results and Gehlen et al. (2003), a timescale analysis and based on that a discussion of our simulations. Our results are not compared with Han et al. (2008), since we have not performed simulations with biological aluminium

incorporation. The last section (5) sums up the conclusions, gives an outline for further development of the model and suggests what further study is needed.

2. Methods

2.1. Model description

To model the three-dimensional distribution of Al_{diss}, the Ocean General Circulation Model (OGCM) called Nucleus for European Modelling of the Ocean (NEMO) is used (Madec, 2008). For this study we use PISCES, one of the biogeochemical components available in NEMO (Aumont and Bopp, 2006; Ethé et al., 2006), which has been employed for many other studies concerning trace metals, as well as large-scale ocean biogeochemistry (Arsouze et al., 2009; Aumont and Bopp, 2006; Dutay et al., 2002, 2009; Tagliabue et al., 2010, 2011). PISCES is run off-line forced by a climatological year of physical fields including subgrid turbulence. The forcing frequency was set to 5 days. These physical fields were calculated by the circulation component of NEMO named OPA (Madec et al., 1998), which was forced by satellite derived wind stress data. Details on the forcings and model configuration can be found in Arsouze et al. (2009) and Dutay et al. (2009).

All input and output fields are defined on the ORCA2 grid, an irregular grid covering the whole world ocean with a nominal resolution of $2^{\circ}\times2^{\circ}$, with the meridional resolution increased near the equator and two 'north poles' in Canada and Russia to eliminate the coordinate singularity in the Arctic Ocean. Its vertical resolution is 10 m in the upper 100 m, increasing downward such that there are 30 layers in total. In Fig. 1 the annually averaged surface velocity field of the OPA output is plotted on the model grid.

It shows the main features of the ocean circulation such as the equatorial current systems, the western boundary currents (Gulf Stream and Kuroshio) as well as the Antarctic Circumpolar Current.

2.1.1. Biogeochemical model

The aluminium cycle (see Section 2.1.2) is implemented in PISCES, a biogeochemical model simulating the cycle of carbon and the major nutrients (nitrate, phosphate, ammonium, silicic acid, and iron), along with two phytoplankton types (diatoms and nanophytoplankton), two zooplankton grazers (micro- and meso-zooplankton), two classes of particulate organic carbon (small and large) of differential labilities and sinking speeds, as well as calcite and biogenic silica. The standard version of PISCES accounts for 24 tracers. For a more detailed description of PISCES see the auxiliary material of Aumont and Bopp (2006).

The aluminium model interacts with the silicon cycle. The model PISCES distinguishes three silicon pools: the silicon content of living diatoms (diatom Si); the silicon content of dead, sinking diatoms (biogenic Si) and dissolved silicic acid. In the model silicic acid and other nutrients are supplied to the ocean by means of atmospheric dust deposition, rivers and sediment mobilisation (Aumont and Bopp, 2006; Gehlen et al., 2007).

2.1.2. Aluminium model

For the modelling of Al, two new tracers are introduced to PISCES: dissolved aluminium (Al_{diss}) and adsorbed aluminium (Al_{ads}). Our Al model follows the approach of Gehlen et al. (2003), i.e., the internal processes (described below) of adsorption and desorption are identical to the model of Gehlen et al. (2003), although the associated biogeochemical model is more complex.

For the standard model configuration, the sole source of Al to the ocean is by dissolution of dust particles in the ocean surface. In one of the sensitivity experiments, a small fraction is also dissolved in the water column (see Section 2.1.4). The used Al:Fe dust fraction of 8.1:3.5 is based on the mass percentages of Al and Fe known to be present in the Earth's crust (Wedepohl, 1995). The solubility of Al from dust is not well constrained, with reported values ranging from 0.5 to 86%, but is probably in the range of 1–15% (Jickells et al., 2005; Measures and Vink, 2000; Orians and Bruland, 1986). Furthermore, it is likely that the source of dust has an impact on the solubility of the Al fraction (Baker et al., 2006; Measures et al., 2010; and references herein). The dissolution of dust is taken as a constant with respect to the origin and location of deposition. The dissolution occurs only in the upper model layer, and is described by the following equation:

$$\frac{\partial}{\partial t}[\mathrm{Al}_{diss}]\bigg|_{z=0} = \alpha\mathcal{D}_{\mathrm{Al}}/H_1, \tag{1}$$

where $\mathcal{D}_{\mathrm{Al}}$ is the Al flux into the ocean, α is the fraction of Al that is dissolved, and H_1 is the thickness of first model layer. Square brackets denote the concentration of the tracer. Since in the mixed layer vertical mixing is rapid, adding Al_{diss} in the first layer is effectively the same as adding it spread out over the mixed layer. The Al that does not dissolve from dust, either at the surface or in the water column, is assumed not to play any role in the biogeochemical cycle of Al on our timescales of interest, and can be thought of as being buried in marine sediments.

Dissolved Al is assumed to adsorb onto biogenic silica particles and, aside from external inputs, the Al_{diss} concentration is essentially governed by adsorption and desorption. The Al_{diss} and Al_{ads} concentrations follow

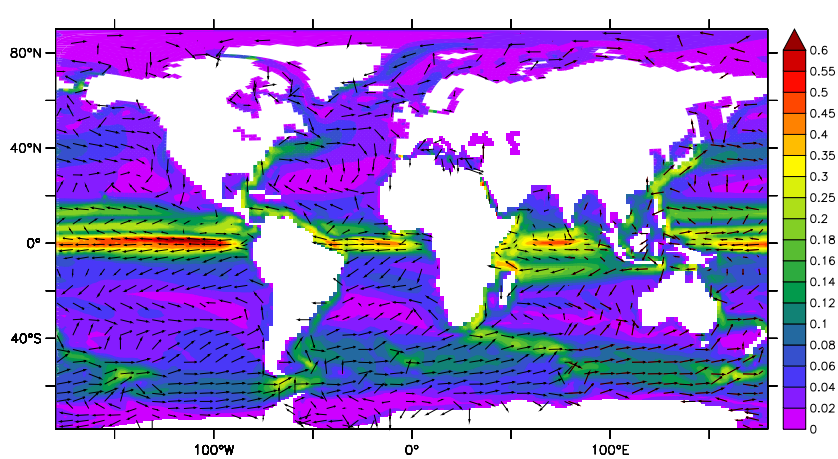

Fig. 1. Velocity at the surface, yearly average. The colour indicates the speed in m/s, while the vectors represent the direction of the flow. Vectors are plotted at every fourth gridpoint.

the following reversible first-order adsorption equation (Gehlen et al., 2003):

$$\frac{\partial}{\partial t}[\mathrm{Al}_{ads}]\bigg|_{adsorption} = \kappa\left([\mathrm{Al}_{ads}^{eq}]-[\mathrm{Al}_{ads}]\right), \tag{2}$$

where

$$[\mathrm{Al}_{ads}^{eq}] = k_{\mathrm{d}}\cdot[\mathrm{Al}_{diss}]\cdot[bSiO_2], \tag{3}$$

in which $bSiO_2$ stands for biogenic silica and $[\mathrm{Al}_{ads}^{eq}]$ is the chemical equilibrium concentration of Al_{ads}. The parameter k_{d} is the partition coefficient and κ is the first-order rate constant for equilibration of Al_{ads} to Al_{ads}^{eq}. Since total Al is conserved when only internal processes are concerned, the time derivative of Al_{diss} is equal to the negative of the time derivative of Al_{ads}.

Eq. (3) describes the chemical equilibrium between Al_{diss} and Al_{ads}, and Eq. (2) illustrates that some time is needed before equilibrium is reached (it is not modelled as an instantaneous process). As noted by Gehlen et al. (2003), this is a purely empirical model and a more mechanistic description of the adsorption/desorption of Al_{diss} onto $bSiO_2$ is difficult, since in reality, the pool of observed "dissolved aluminium" is operationally defined, i.e., it exists as different kinds of ions as well as colloids that can go through a filter of, e.g., 0.2 μm. Also the adsorbent, $bSiO_2$, exists in various forms and it is, for instance, difficult to even define the charge density, which is important for its potential to adsorb Al_{diss}. Usually the surface is covered by natural organic matter (Filella, 2007; Lead and Wilkinson, 2007).

Furthermore, the main scavengers for aluminium in the open ocean also include particulate organic matter (POM), calcium carbonate ($CaCO_3$) and even particulates that are not part of PISCES (such as lithogenic particles that do not participate actively in biogeochemical cycles). Hence it is difficult to conceive a mechanistic model of ad- and desorption of "Al_{diss}" onto the poorly defined pool of particulates.

In our model only $bSiO_2$ is used as a scavenger of Al_{diss}. Biogenic silica is likely to be the most important because (1) it sinks quickly, so that Al has little chance to significantly desorb from $bSiO_2$ (ballast effect), and (2) positively charged aluminium ions are easily adsorbed onto the negatively charged surface of $bSiO_2$ particles (Dixit and Cappellen, 2002; Loucaides et al., 2010).

Sinking of $bSiO_2$ and Al_{ads} is described as follows. In the model, $bSiO_2$ sinks with a speed of $w_{\mathrm{ML}}=30$ m/day in the mixed layer. Below the mixed layer, it increases linearly with depth, reaching a value of $w_{4\mathrm{km}}=200$ m/day at 4 km below the mixed layer (Aumont and Bopp, 2006). This means that Al_{ads} also sinks with this speed, while it can desorb following Eqs. (2) and (3). For every layer in the model, the following equation holds:

$$\frac{\partial}{\partial t}[\mathrm{Al}_{ads}]\bigg|_{\mathrm{sinking}} = -\frac{\partial}{\partial z}\left(w_s\cdot[\mathrm{Al}_{ads}]\right), \tag{4}$$

where w_s is the sinking speed, given in the mixed layer by a constant w_{ML} and below the mixed layer increasing with depth according to:

$$w_s = w_{ML} + (w_{4km}-w_{ML})\cdot\frac{z-D_{ML}}{4000m-D_{ML}}, \tag{5}$$

where z is the model depth. Once sunk to the ocean floor, we assume that the aluminium is buried permanently. This is described by the following change of Al_{ads} in the bottom layer: $\frac{\partial}{\partial t}[\mathrm{Al}_{ads}]\Big|_{z_{sed}} = -[\mathrm{Al}_{ads}]\cdot w_s/H_{sed}$, where H_{sed} is the thickness of the bottom model layer.

Adding advection and mixing, the full equations for $[\mathrm{Al}_{ads}]$ and $[\mathrm{Al}_{ads}]$ away from the boundaries are as follows:

$$\frac{\mathrm{d}}{\mathrm{d}t}[\mathrm{Al}_{ads}] = \kappa\left([\mathrm{Al}_{ads}^{eq}]-[\mathrm{Al}_{ads}]\right)-\frac{\partial}{\partial z}\left(w_s\cdot[\mathrm{Al}_{ads}]\right)+\left(\mathcal{A}\nabla_H^2+\nu_E\frac{\partial^2}{\partial z^2}\right)[\mathrm{Al}_{ads}], \tag{6}$$

$$\frac{\mathrm{d}}{\mathrm{d}t}[\mathrm{Al}_{diss}] = -\kappa\left([\mathrm{Al}_{ads}^{eq}]-[\mathrm{Al}_{ads}]\right)+\left(\mathcal{A}\nabla_H^2+\nu_E\frac{\partial^2}{\partial z^2}\right)[\mathrm{Al}_{diss}], \tag{7}$$

where the general advection ($\mathbf{v}\cdot\nabla$) of the tracers is implicit in the full time derivatives. $\mathcal{A}$ and ν_E are the horizontal and vertical eddy diffusivity coefficients, respectively.

The code of the NEMO model, as well as PISCES and the aluminium model, is free software: software that can be used, studied, and modified without restriction (except that published modifications must fall under the same license). It is available at http://www.nemo-ocean.eu/. Version 3.1 of the NEMO model is used, specifically svn revision 1183. This can be accessed through http://forge.ipsl.jussieu.fr/igcmg/svn/modipsl/. The aluminium specific code is available under the same conditions as an electronic supplement to this article: trcal_sed.F90 describes aluminium deposition into the ocean and into the sediment, and trcal_rem.F90 describes the internal processes of ad- and desorption.

2.1.3. Input fields

The dust deposition field was taken from the output of the INCA model, an atmospheric dust model (Whitehead et al., 1998). INCA is the aerosol module of the LMDzT atmospheric model (Schulz et al., 2009). The resulting climatology is used and described by Aumont et al. (2008) and evaluated by Textor et al. (2006). The surface deposition is shown in Fig. 2(a). Most dust is deposited in the Atlantic Ocean, just west of the Sahara and just west of the Kalahari Desert. Another important dust deposition site is found in the northern Indian Ocean. Dust deposition east of Asia in the Pacific Ocean is much smaller, and in the South Pacific Ocean, the Southern Ocean and the Arctic Ocean there is almost no deposition of dust. The amount of dust per basin is listed in Table 1.

According to Textor et al. (2006) the model that is used to create this dust deposition field is validated against high-quality observational datasets, but there are a number of uncertainties, because there are not enough observations available to sufficiently constrain any dust model globally. The spatial resolution is nominally 2°, and the temporal resolution is 1 month (12 time steps per year). In reality, dust deposition is highly sporadic (Aumont et al., 2008; Rijkenberg et al., 2008). Dust events are expected to be highly local and there is sufficient horizontal mixing to dilute the Al_{diss} distribution, such that there is no significant concentration change. This has also been observed in the North Atlantic Ocean (Rijkenberg, 2012). Furthermore, our aim is to look at averages of $[\mathrm{Al}_{diss}]$ over at least several months, and therefore it is acceptable to use monthly averaged dust deposition fields.

The deposition field (Fig. 2(a)) is very similar to the one used by Jickells et al. (2005), except that in our field there is almost no dust deposition near Argentina and Chili. In Fig. 2(b) the sediment source is plotted, which is used for one of the sensitivity experiments. It is a function developed for Fe fluxes and depends on the sea floor topography (which accounts for the degree of oxygenation of the sediments), as described by Aumont and Bopp (2006). The Al:Fe mass ratio used is 8.1:3.5, the same as for the dust deposition field.

2.1.4. Simulations

Our goal in this study is to better understand how the assumptions made in our model impact on the distribution of Al_{diss}. Specifically, we aim to examine the importance of different Al cycle processes and

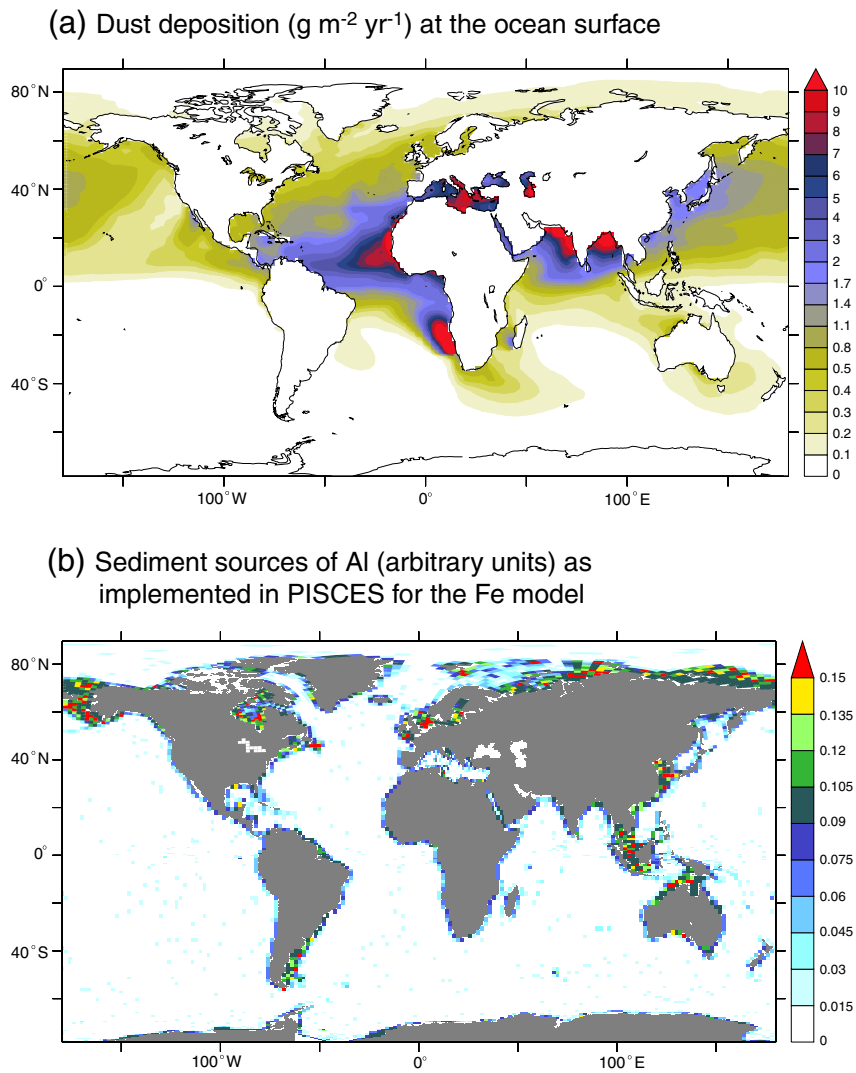

Fig. 2. Aluminium sources used to force the model, based on the Fe input in PISCES, using an Al:Fe crustal ratio of 8.1 : 3.5.

external Al_{diss} sources. To that end, five sensitivity experiments are performed (see Table 2) with parameters different from the reference experiment.

For the reference experiment a 5% dissolution of the Al fraction is used, which is within the known range and close to the values used by Gehlen et al. (2003) (3%) and Han et al. (2008) (5%). The partition

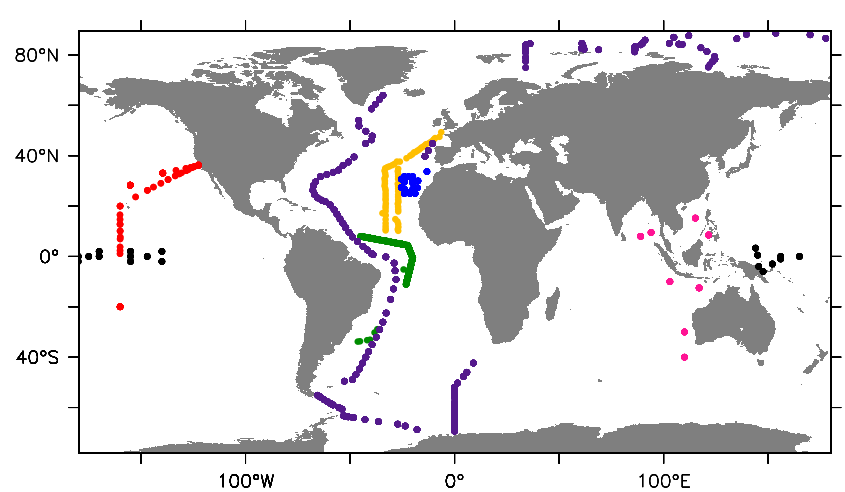

Fig. 3. Stations of the cruises: M 60 [yellow]; MC-80 and VERTEX [red]; IOC96 [green]; IRONAGES III [blue]; KH-98-3 [pink]; EUCFe [black]; Geotraces-NL [purple]. See Table 3 for an overview with references and the number of observations.

Table 1
Amount of yearly dust and sediment input in each basin. The Southern Ocean is defined as the ocean south of 59°S, without overlap with the Pacific, Atlantic and Indian Oceans.

Basin	Dust deposition		Sediment sources
	Absolute (Tg/year)	Relative (%)	Relative (%)
Atlantic Ocean	128.3	47.9	18.1
Indian Ocean	58.3	21.8	7.4
Pacific Ocean	54.3	20.3	27.9
Southern Ocean	0.3	0.12	11.4
Arctic Ocean	1.5	0.55	22.8
Mediterranean Sea	17.8	6.6	3.6
other seas	7.4	2.8	8.9
Total	267.9	100.0	100.0

Table 2
Overview of reference and sensitivity experiments. Deviations from the reference experiment are in bold.

Experiment	Surf. diss. (%)	Subsurf. diss.	k_d (10^6 l/kg)	κ (year^{-1})	Sediments
Gehlen et al. (2003)	3	No	1	10000	No
Han et al. (2008)	5	No	–	–	No
Reference experiment	5	No	4	10000	No
Doubled dissolution	**10**	No	4	10000	No
With subsurface diss.	5	**Yes**	4	10000	No
With ocean margins	5	No	4	10000	**Yes**
Halved part. coeff. k_d	5	No	**2**	10000	No
Slow-equilibration κ	5	No	4	**100**	No

coefficient k_d is set at $4 \cdot 10^6$ l/kg. This quantity signifies the amount of Al that can adsorb onto biogenic silica particles, which means that if k_d is to be increased, Al_{diss} is exported in larger quantities by scavenging. Our value is four times higher than that of Gehlen et al. (2003), but much smaller than the one used by McAlister and Orians (2011) ($5.6 \cdot 10^7$ l/kg, used for shelves as well as open ocean regions).[1] The first-order rate constant κ, which signifies how quickly the equilibrium between Al_{diss} and Al_{ads} is established, is not constrained by the literature.

All these parameters for the reference experiment are chosen in such a way that the model simulates the Al_{diss} distribution from the observations of the selected cruises (see Section 2.2) reasonably well, while all the parameters remained within literature ranges.

After 600 years the reference experiment is forked into several sensitivity simulations. These sensitivity experiments are run, along with the reference experiment, for another 1300 years or more to a steady state. The total model time for the reference simulation is 2200 years. An overview of all key parameters for the simulations is given in Table 2.

For all experiments we use the OPA physical fields and atmospheric dust deposition as described in Section 2.1.3. In all simulations, except for the third which tests the sensitivity of water column dissolution, Al is dissolved only in the surface ocean. In the third experiment Al is dissolved in the water column as well with the fraction $10^{-4} \cdot e^{-z/z_0}$ of the dust deposition field, where z is the depth in km and $z_0 = 1$ km. The extra term added to Eq. (7) is $\tilde{\alpha} \cdot e^{-z/z_0} \mathcal{D}_{Al}/H_k$, where H_k is the thickness of layer k and $\tilde{\alpha}$ forms with the exponent the fraction of Al that is dissolved in layer k.

The sensitivity simulations can be divided into two types of sensitivity experiments: the first three test the sensitivity to Al sources (amount of dust dissolution into the surface ocean and into the ocean water column, and the inclusion of ocean sediment dissolution) and the last two test the sensitivity to the internal Al cycling (lower partition coefficient k_d and lower first-order rate constant κ).

2.2. Observations

The recent IPY-Geotraces observations in the Arctic (Middag et al., 2009), North-east Atlantic (Middag, 2010, Chapter 5), West Atlantic (Middag et al., in preparation) Oceans and the Atlantic section of the Antarctic Ocean (Middag et al., 2011) are used for a detailed comparison and optimisation of the model parameters. See the upper part of Table 3 for these datasets and Fig. 3 for the station positions. These datasets comprise overall 3455 individual data values for dissolved Al. All values have been verified versus international reference samples and their consensus values of the SAFe and Geotraces programmes, see supplementary material S-1. Moreover, during cruise 64 PE 321 (2010) excellent agreement was obtained for a complete vertical profile of dissolved Al at the BATS station between a previous occupation and dissolved Al data in 2008 by the US Geotraces group, see supplementary material S-2. This large amount of observations give the possibility to compare the model with deep ocean observations of [Al_{diss}], allowing us to validate the model in the deep ocean and to study the global Al cycle in more detail.

For a worldwide global ocean comparison one has to rely on data that was collected in the era before the reference samples of SAFe and Geotraces were available. Inevitably the definition of criteria for selecting such previously published datasets is less rigorous, see Electronic supplement S-3 for the criteria used for each of the selected datasets. The selected datasets are listed in Table 3, lower part, and positions are shown in Fig. 3.

3. Results

3.1. Reference simulation

Our reference experiment is performed for a spin-up period of 2200 years. The resulting total ocean Al budget in the reference simulation is around 7 Tmol (1 Tmol = 10^{12} mol). Already after 600 years the total Al distribution is more or less in a steady state as shown by Fig. 4, where the total integrated aluminium (dissolved and adsorbed) is plotted against time. Therefore, from 600 years our sensitivity experiments (see Section 3.2) are forked. The relevant tracers of the raw model output can be found at http://data.zkonet.nl/index.php?page=Project_view&id=2916&tab=Datasets.

Fig. 5 shows the Al_{diss} surface concentration of the reference experiment. As in all subsequent plots, yearly averages are shown. There is a seasonal cycle in [Al_{diss}] in our model, but it is small relative to the spatial trends. The observed Al_{diss} concentrations from our Al data compilation (see Section 2.2) are plotted as circles over the model Al_{diss} concentration in this and later figures. A comparison of the model with the observations will be done in Section 3.1.1. Consistent with the dust deposition field (Fig. 2(a)), the largest modelled Al_{diss} surface concentrations are in the central Atlantic Ocean, with values between 30 and 40 nM (1 nM = 10^{-9} mol/l) near 20°N, decreasing northward to values in the order of several nM north of 60°N. The concentration of Al_{diss} between 40°N and 60°N is larger than expected based on the dust deposition field (Fig. 2(a)). This is because the Gulf Stream and the North Atlantic Current transport Al_{diss} northward before most of it is scavenged. As will be shown in Sections 4.2.1 and 4.5, most Al_{diss} is scavenged before it passes Iceland. The result is that [Al_{diss}] in the surface waters of the Arctic Ocean is in the order of 1 nM. On the other side of the globe, south of 40°S, the Al concentration is even lower, less than 1 nM. This is to be expected on the basis of [$bSiO_2$] (Fig. 6) and the dust deposition flux (Fig. 2(a)). In the Pacific Ocean the concentration is relatively

[1] We did not use the k_d value from Gehlen et al. (2003), because initial experiments showed that this would leave too much Al_{diss} in the ocean surface, especially at high latitudes.

Table 3
Observational data used for comparison with model. For positions see Fig. 3.

Cruise	Research vessel	Year	Location	Source	Nr. of data
ARK XXII/2	Polarstern	2007	Arctic	(Middag et al., 2009)	1080
ANT XXIV/3	Polarstern	2008	Southern Ocean	(Middag et al., 2011, 2012)	919
64 PE 267	Pelagia	2007	North-east Atlantic	Middag et al.	137
64 PE 319	Pelagia	2010	North-west Atlantic	Middag et al.	383
64 PE 321	Pelagia	2010	Centre-west Atlantic	Middag et al.	504
JC057	James Clark Ross	2011	South-west Atlantic	Middag et al.	432
Subtotal used primarily for detailed comparison and optimisation of the model					3455
Compilation of selected other observations for global ocean comparison:					
IOC96	Knorr	1996	Central-south Atlantic	(Vink and Measures, 2001)	1049
M 60	Meteor	1982	North-east Atlantic	(Kremling, 1985)	91
IRONAGES III	Pelagia	2002	North-east Atlantic	(Kramer et al., 2004)	181
EUCFe	Kilo Moana	2006	Equatorial Pacific	(Slemons et al., 2010)	195
MC-80	Thompson	1980	Pacific	(Orians and Bruland, 1986)	92
VERTEX-4	Wecoma	1983	North Pacific	(Orians and Bruland, 1986)	54
VERTEX-5	Thompson	1984	North Pacific	(Orians and Bruland, 1986)	59
KH-98-3	Hakuho-Maru	1996	East Indian	(Obata et al., 2007)	152
Subtotal compilation of selected other observations for global comparison					1873
Grand total of all dissolved Al values used in this study					5328

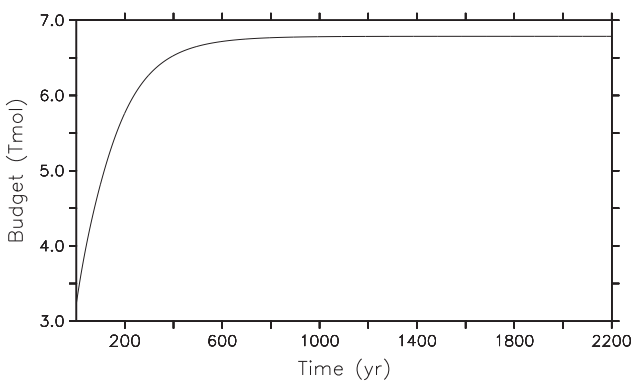

Fig. 4. Total Al budget ($[Al_{ads}]+[Al_{diss}]$) (Tmol) in the world ocean, plotted against the model years.

low as well, except near 20–35°N where a wide band of high $[Al_{diss}]$ can be found.

This maximum arises from the large dust deposition along the Asian continental margin between 20°N and 60°N. North of 40°N, the concentration of $bSiO_2$ is high, as can be seen in Fig. 6. Therefore, in that region the dissolved Al is quickly depleted by the high $bSiO_2$ concentration in the surface, while south of 40°N the North Pacific Current transports it eastward into the central North Pacific Ocean.

In Fig. 7 the modelled Al_{diss} concentration of the reference experiment is shown at selected depths (100, 500, 1000 and 3000 m) and in Fig. 8 the Geotraces cruise section in the West Atlantic Ocean. This section was calculated from the three-dimensional model data by converting the ORCA2 gridded model data to a rectilinear mapping and after this interpolating the rectilinear data onto the cruise track coordinates.

In the Atlantic Ocean there is a maximum of $[Al_{diss}]$ from about 30°S at 2 km depth, getting higher northward (Fig. 8). According to the model, deep Al_{diss} concentrations are low in the Southern Ocean, the Arctic Ocean and the Pacific Ocean (Fig. 7).

3.1.1. Comparison with observations

In Figs. 5, 7 and 8 observed Al_{diss} concentrations (see Section 2.2) are plotted as circles over the modelled results. The precision of the measurements performed during the Geotraces cruises at a 1 nM level and lower (polar oceans) was about 4% and at a 20 nM level (West Atlantic Ocean) about 2% (Middag, 2010, p. 25). These observations have a standard deviation that is smaller than can be distinguished based on the colour bar. Older observations generally have lesser precision, but are of sufficient quality (see Section 2.2). Therefore the model results can in principle be compared with the observations without regard of measurement errors.

Fig. 5 shows that the model and the observations reveal similar patterns in the surface ocean: high concentrations in the central

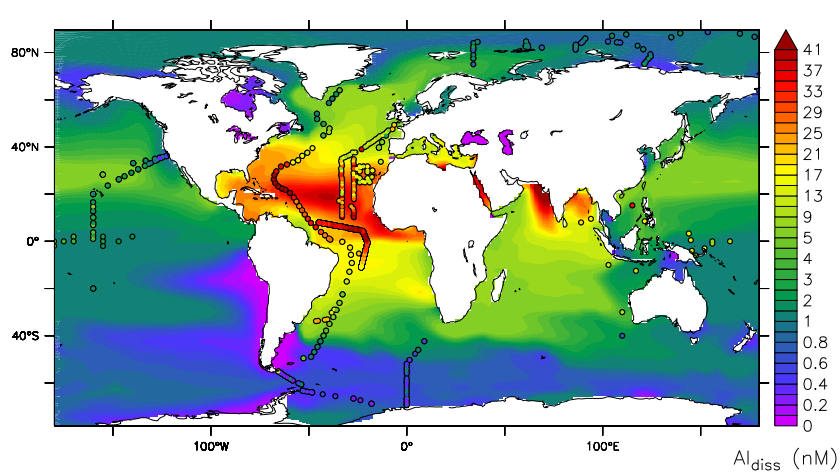

Fig. 5. Dissolved aluminium concentration (nM) from the reference experiment at the surface ocean, with respective observations plotted on top of it. Note that the scale is expanded for low concentrations.

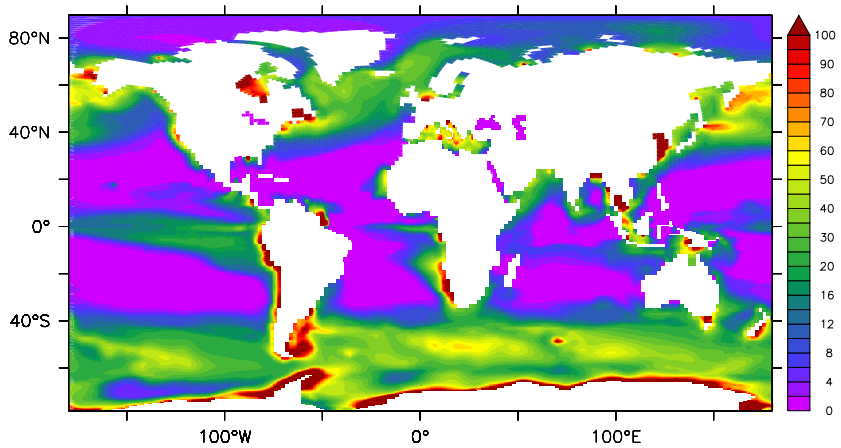

Fig. 6. Biogenic Si concentration (nM) in the PISCES model, at the surface, yearly average.

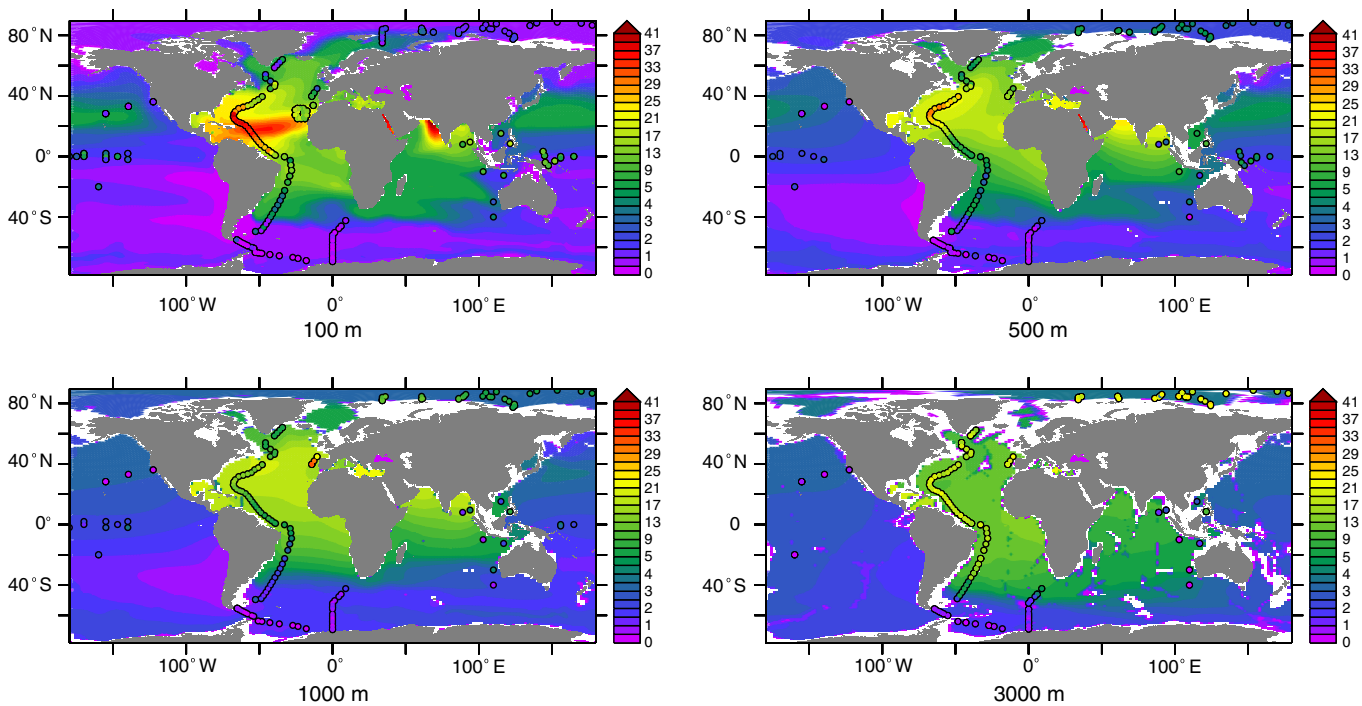

Fig. 7. Dissolved aluminium concentration (nM) from the reference experiment at several depths, with respective observations plotted on top of it.

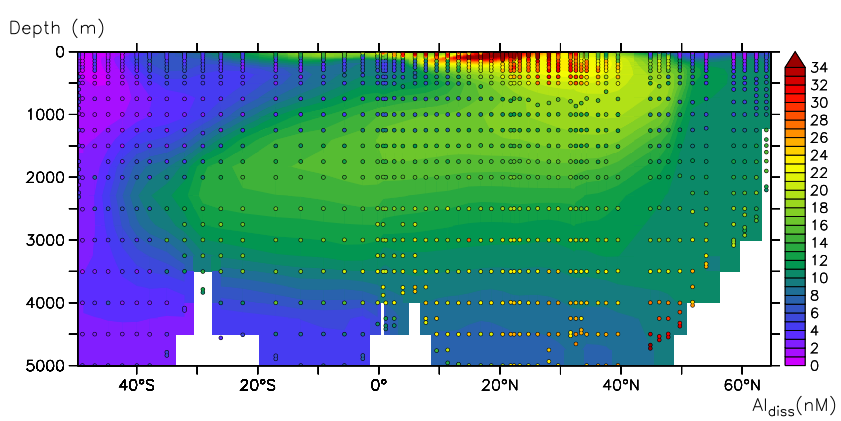

Fig. 8. Dissolved aluminium (nM) from reference experiment along the West Atlantic Geotraces cruise track. Observations are plotted on top.

Atlantic Ocean and low concentrations in the polar oceans and the Pacific Ocean. However, details in the modelled Al_{diss} distribution do not agree with the observations. For instance, the large concentration in the Pacific Ocean between 20 and 35°N is not visible in the observations of Orians and Bruland (1986).

Also between 45 and 65°N in the West Atlantic Ocean the concentration of Al_{diss} in the model is overestimated compared with the Geotraces observations near Greenland (Middag et al., in preparation). This suggests that Al is not sufficiently scavenged in this area. This is further discussed in Section 4.2.

The model underestimates [Al_{diss}] near Brazil. This can be related to errors in ocean currents (Fig. 1), as the transport of low [Al_{diss}] water might be too high in the Brazil current. In reality this current is narrower than the 2° resolution of the model. Another possibility is that the dust deposition field is not realistic in this area.

Furthermore, the observations generally have more spatial variability than the modelled [Al_{diss}]. Many of these differences depend on several model boundary conditions (dust deposition distribution, velocity field, particle sinking speed) as well as temporal variability, because the model results plotted are yearly averages, while observations are done throughout the year in precise locations.

Fig. 8 shows that similar patterns are present in the West Atlantic Ocean in the model and the observations. There is a clear pattern of North Atlantic Deep Water (NADW), which is mainly visible between 40°S and 20°N in both the model and the observations. In Fig. 9 the Atlantic Overturning Stream Function (OSF) is plotted over the model results, showing that the patterns of the OSF and [Al_{diss}] coincide. In the Southern Ocean, low concentrations of Al_{diss} in the upper km are clearly penetrating from the Southern Ocean northward to at least 20°S around 500 m depth. This is Antarctic Intermediate Water (AAIW) and Subantarctic Mode Water (SAAMW). From the Southern Ocean near the bottom, there is also Antarctic Bottom Water (AABW) flowing northward, visible in the observations and the model.

The similarity between the model and the observations lessens in the deeper North Atlantic Ocean, where according to the observations [Al_{diss}] increases with depth (for depths below 800 m), while in the model there is a decrease with depth below 1.5 km. Besides this general pattern of increase of [Al_{diss}] with depth in the observations, a very high concentration of Al_{diss} is present between 45 and 50°N near the sediment, which enhances the dissimilarity between the model and the observations. This problem will be discussed further in Section 4.5.

Furthermore, in the southern hemisphere in the model the maximum of [Al_{diss}] is at about 2 km depth, indicating a southward flow around 2 km depth. In the observations this maximum is at 3 km depth, indicating a southward flow at 3 km depth. Indeed, according to the hydrographical analysis of the West Atlantic Geotraces cruise (van Aken, 2011) the flow is at 3 km depth. As can be seen in Fig. 9 the southward flow is too high in the water column compared to the observations.

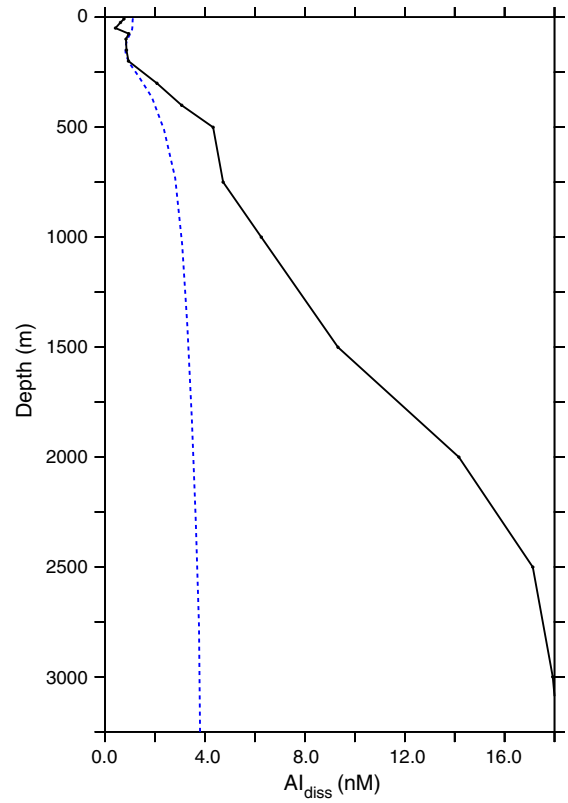

Fig. 10. [Al_{diss}] (nM) profile in the eastern Arctic of reference experiment (blue dashed line) and the observations of IPY-Geotraces-NL observations (black solid line) at 213.6°E, 87.03°N.

Another feature which is not captured by the model is the aluminium profile in the eastern Arctic Ocean, which is shown in Fig. 10. It shows that the model [Al_{diss}] increases with depth from a minimum near 150 m to a maximum near the bottom by a factor of 3 (and is in the order of 2 nM, see Fig. 10). The observations show an increase as well (as also presented in Fig. 7), but here it is far more pronounced with a small minimum at the surface (less than 1 nM) to a large maximum near the abyss (around 18 nM) (Middag et al., 2009). Thus in the Arctic Ocean the vertical change in [Al_{diss}] in the model is by far not as pronounced as in the observations. The absence of sediment sources of Al might play a role in this. The results of a simulation with sediment sources will be discussed in Section 3.2.3.

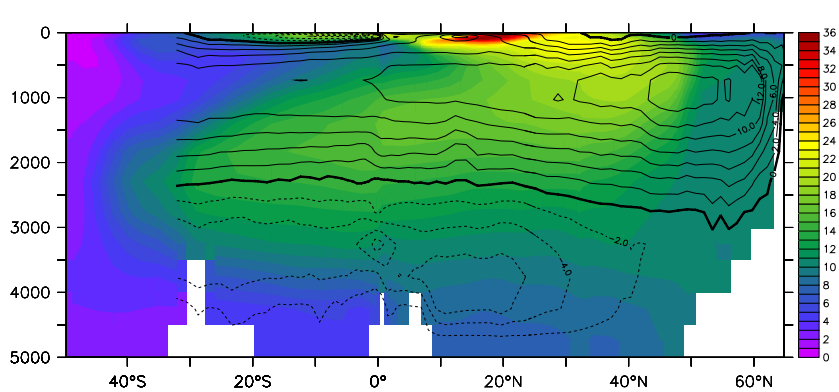

Fig. 9. The quantity in the coloured area is the model [Al_{diss}] (nM) at the Geotraces West Atlantic cruise section. The contours represent the model Atlantic Overturning Stream Function (Sv).

3.2. Sensitivity simulations

Section 2.1.4 described how our sensitivity simulations are set up. The reasons why we performed these specific experiments are closely related to the problems we encountered while interpreting the results from the reference experiment (Section 3.1). After a brief summary of two of these problems and associated sensitivity simulations, the results of these simulations will be presented. The relevant tracers of the raw model output can be found at ftp://zkoclient:zko@dmgftp.nioz.nl/zko_public/00056.

How can it be that in the Atlantic Ocean from 800 m depth to the bottom of the ocean there is a decrease in the Al_{diss} concentration in the model, while according to the observations there is an increase (see Fig. 8)? The only transformation mechanism in our model is reversible scavenging, which should give a profile where [Al_{diss}] increases with depth, and the only source is dust. However, the model biogenic silica concentration, its sinking speed, advection and mixing, and the first-order rate constant κ are all relevant for the vertical distribution of Al_{diss} as well. Since the biogenic silica concentration and the physical fields can both be assumed to be reasonably realistic (see Section 2.1), no sensitivity simulations concerning these fields are described in this paper. We do perform one simulation with a different first-order rate constant (Section 3.2.5) to investigate where in the ocean this parameter influences the Al_{diss} distribution. The value of κ is significantly decreased in this simulation (this parameter is very poorly constrained by observations).

Concerning the strongly depth-increasing profile of Al_{diss} as observed in the eastern Arctic Ocean (Fig. 10), we perform a simulation where sediment ocean margins are added as a source of Al_{diss}, following the approach of (Aumont and Bopp, 2006) and assuming an Al:Fe fraction of 8.1:3.5 in the sediments (thus we assume sediment Al_{diss} supply is coupled to Fe). The result of this simulation is discussed in Section 3.2.3. Furthermore, an experiment is performed where the partition coefficient is decreased from $4 \cdot 10^6$ l/kg to $2 \cdot 10^6$ l/kg, which is a way to evaluate the importance of relative partitioning between the dissolved and adsorbed fraction. This experiment will be discussed in Section 3.2.4.

3.2.1. Increased dust dissolution fraction

To examine the impact of greater dust dissolution on the cycling and distribution of Al_{diss}, we increase the surface dissolution percentage of Al from 5 to 10% ('doubled dissolution'). In Fig. 11 the resulting change in [Al_{diss}] in the surface ocean. In the West Atlantic Ocean along the Geotraces cruise track the increase in [Al_{diss}] is everywhere between 99 and 100% (not plotted). The [Al_{diss}] is increased with a factor of two in most locations in the ocean. The doubling can be explained when the model equations (Eqs. (2) and (3)) are considered.

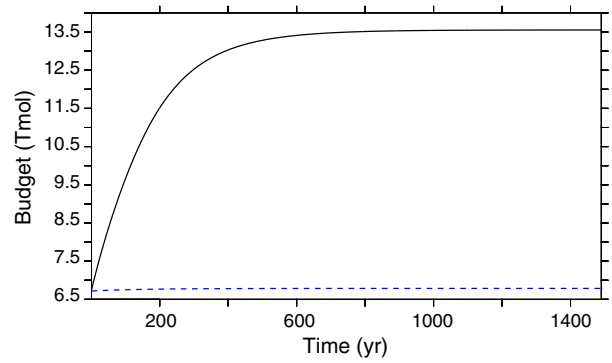

Fig. 12. Total Al budget (Tmol) in world ocean during spin-up of 1490 years for increased dissolution sensitivity simulation (solid black line; forked from the reference simulation at year 600). The dashed blue line signifies the Al budget of the reference simulation.

Consider a one-box model in which equilibration is instantaneous ($\kappa = \infty$). If we increase dust dissolution everywhere with a factor of two and wait until steady state, we also get a doubled particulate Al burial. This means that [Al_{diss}] must be doubled in the ocean since the sinking/burial speed does not change. Since in steady state [Al_{ads}] is proportional to [Al_{diss}] (Eq. (3)), [Al_{diss}] must be doubled as well. Hence a doubled [Al_{diss}] is expected. In other words, the total Al budget is linear with the input. (See for instance Broecker and Peng, 1982 for background.) This means that the amount of dissolution in the surface ocean has an effect everywhere in the ocean, i.e. the effect is global and not restricted to dust deposition sites.

The Al budget is not doubled everywhere. Fig. 11 shows that in the coastal upwelling region near Chili the increase is only around 95%. This is because the model is not completely spun up, as can be seen in Fig. 12, so that the increased dissolution of Al from dust has not reached the deep Pacific Ocean yet. Therefore the percentages in Fig. 11 indicate how close the subsequent sensitivity simulations are to steady state in different regions in the ocean.

3.2.2. Water column dust dissolution

For the reference experiment we included dust dissolution only in the surface ocean to assume that Al from dust only dissolves in the surface ocean. During sinking of dust more Al might be dissolved. To test the effect of water column dissolution we performed a sensitivity simulation with water column dissolution included.

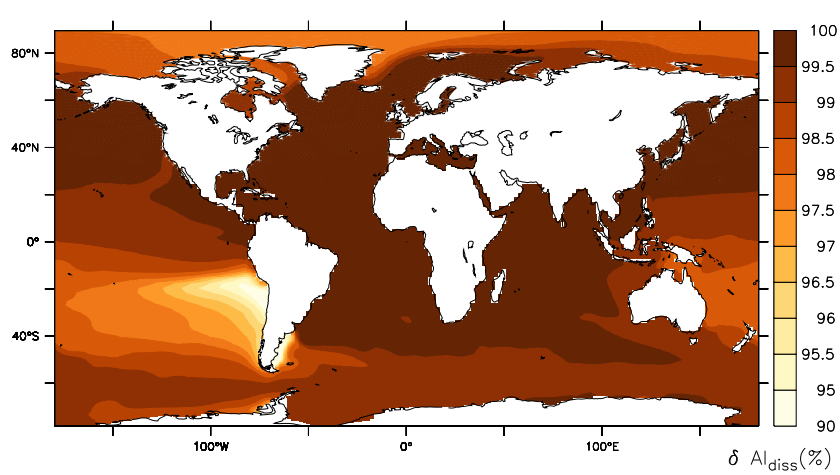

Fig. 11. The relative surface difference of the dissolved aluminium concentration between the experiment with an increased dissolution (10%) and the reference experiment (5% aluminium dissolution). The scale is in percentages, of which the largest part from 95% to 100%.

Gehlen et al. (2003) have included Al_{diss} input at the surface only, but they do compare different dust deposition distributions, as do Han et al. (2008). The latter also dissolve dust below the surface layer, but no sensitivity experiments have been presented for water column dissolution. None of our sensitivity experiments, as part of an OGCM, have been published before.

Our simulation with water column dissolution resulted in slightly higher values of [Al_{diss}] of up to 0.7 nM more in some places. Fig. 13 compares [Al_{diss}] in the water column dissolution experiment with the reference experiment (Figs. 5 and 8).

On first sight, north of the equator, water column dissolution moves the modelled [Al_{diss}] away from the observations. This is clear if the decrease in [Al_{diss}] with depth is considered in the reference simulation, while in the observations [Al_{diss}] increases with depth. The simulation with water column dissolution makes the modelled decrease even more pronounced. Also the high [Al_{diss}] in the upper 500 m is only slightly improved, and not at precisely the right location: in the upper 500 m the model especially underestimates [Al_{diss}] between 20 and 35°N. Therefore, water column dissolution does not improve the model results.

3.2.3. Ocean sediments source

It is possible that dissolution of dust is not the only way in which aluminium enters the ocean. River input and hydrothermal vents are excluded as significant sources of Al (see Section 1). But one other source that might be significant, and might also help our model to produce more realistic [Al_{diss}] (e.g. in the Arctic Ocean), is redissolution of Al from sediment resuspension. Therefore, in one of the simulations, we have included a rough approximation of Al margin sources, as described in Section 2.1.3. The resulting [Al_{diss}] and its difference with the reference experiment are plotted in Fig. 14.

The influence of shelf sediment sources on the aluminium distribution can clearly be seen. Especially in the Arctic Ocean, the Indonesian Archipelago and near the east coast of North America, dissolved aluminium is increased substantially when sediment input is added to the model. This is to be expected, since the largest sediment source is on the shelf areas (see Fig. 2(b) for the added Al source).

Let's now look at the West Atlantic cruise track. Fig. 14(c) represents the difference between the sediment source experiment and the reference simulations at the ocean surface. There is a clear increase at and near the surface between 20 and 40°N in the West Atlantic Ocean.

The cruise section difference plot in Fig. 14(d) shows a large increase in the NADW. So it seems that high [Al_{diss}] can be explained by not only dust deposition but also sediment sources. This is consistent with the explanation of (Middag et al., in preparation), even though their arguments mostly concern deep sediment resuspension and to a lesser extend margin sediments. The sediment source in our model is mostly from near-shore sediment resuspension (Fig. 2(b)), in line with the findings of Mackin and Aller (1986). Of course, a deep sediment source might also explain the high [Al_{diss}] near the sediment at 45–50°N, and it may therefore be important to include such a source in a future model study, since our current results suggest that margin sediments do not effectively reproduce this maximum.

The concentration in the model gets significantly higher in the Arctic Ocean which is bad for depths between the surface and a few km, but

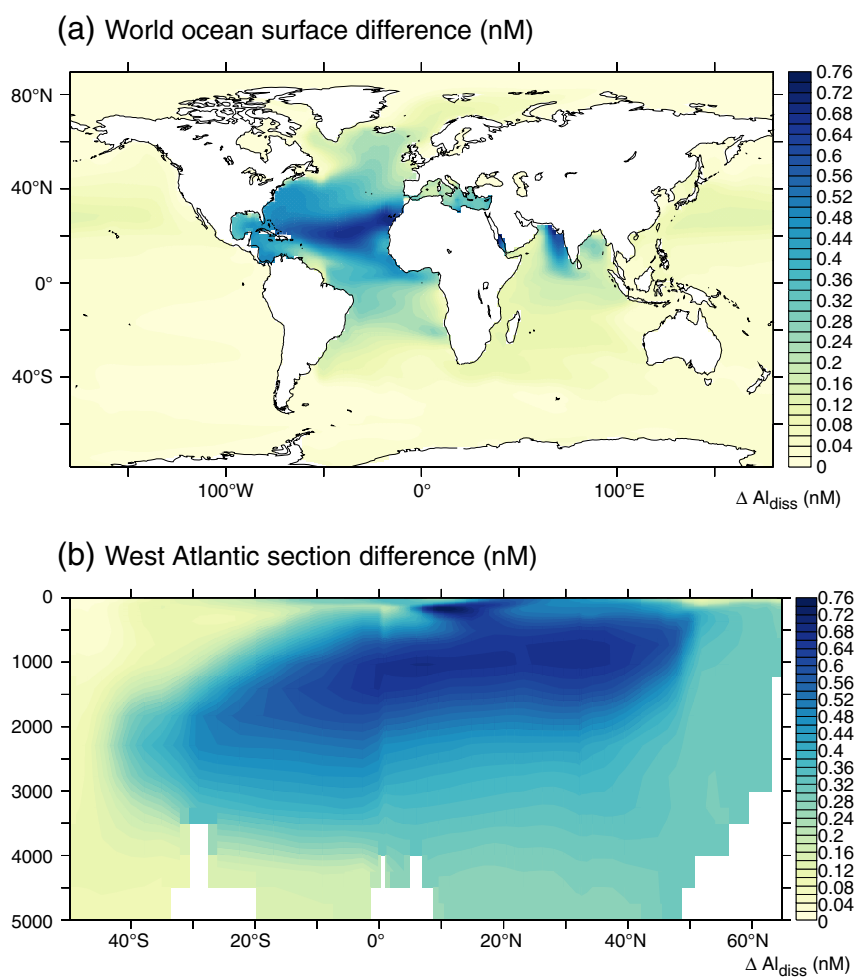

Fig. 13. Difference in [Al_{diss}] (nM) between the simulation with water column dissolution with the reference simulation (without water column dissolution).

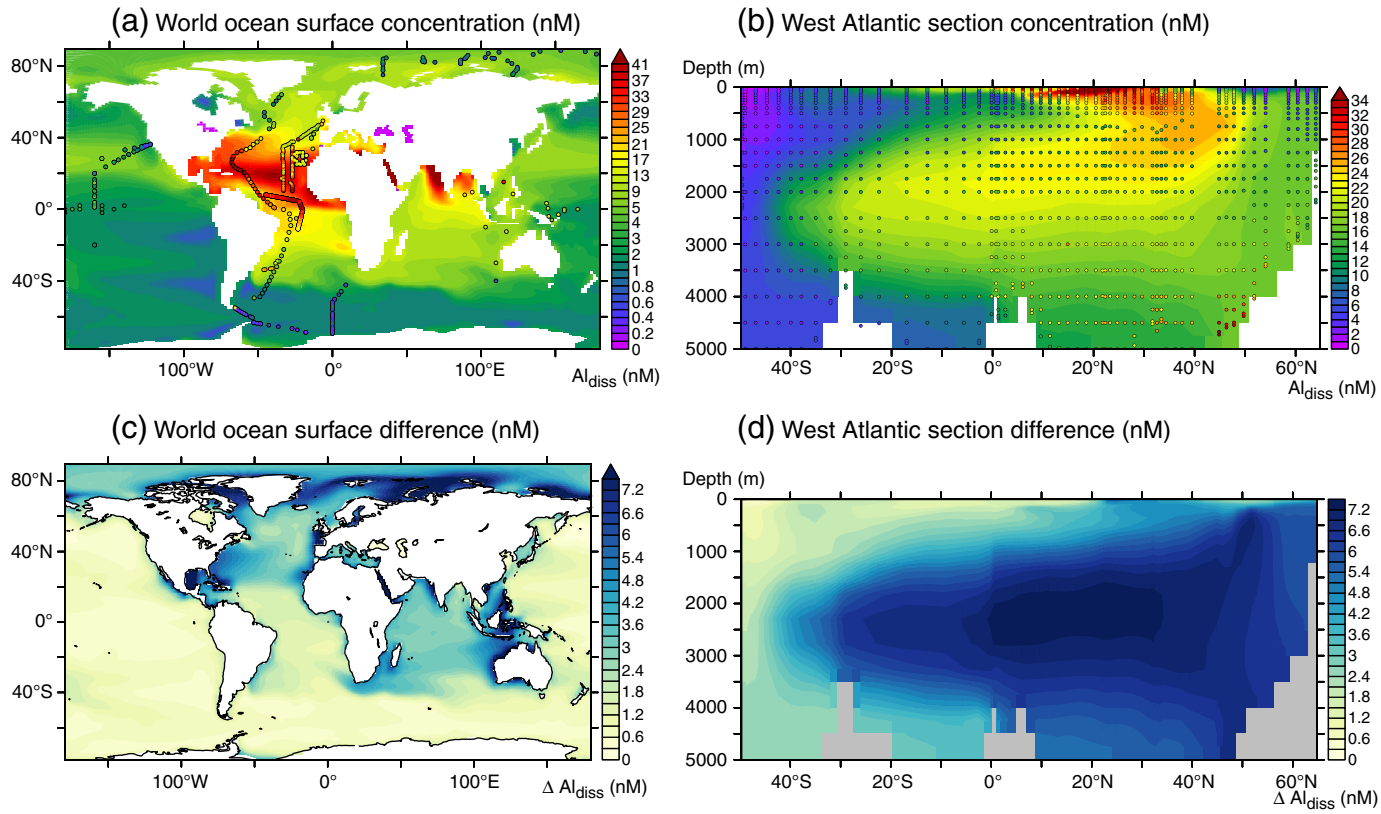

Fig. 14. Experiment with sediment input: [Al_{diss}] (a and b) and its difference with the reference run (c and d).

better for deeper waters, where a much higher concentration of aluminium was observed. This is shown in the profile plots of Fig. 15.

3.2.4. Decreased partition coefficient

One of the key parameters in our model is the partition coefficient k_d. It regulates the amount of Al that can be adsorbed by $bSiO_2$. To see what effect this parameter has in our model setup, we performed an experiment in which k_d is decreased by a factor of two.

Fig. 16 shows that a decrease of k_d leads to the most significant relative increase of [Al_{diss}] in the Southern Ocean.

3.2.5. Decreased first-order rate constant

The second most important scavenging parameter is the first-order rate constant κ. This parameter should have a dynamic effect on the distribution of Al_{diss}, since it describes how quickly Al_{diss} and Al_{ads} equilibrate (see Eq. (3)). To test this in our model, we decreased κ from 10^4 to 10^2 year^{-1}.

As can be seen in Fig. 17, surface [Al_{diss}] increases significantly compared with the reference experiment (compare Fig. 5 with Fig. 17(a)). Fig. 17(d) shows the relative change in [Al_{diss}] in the West Atlantic Geotraces section. From the equator northward below 2 km depth an increase of aluminium is visible. There is also an increase near the deep sediment between 45 and 50°N, but it is too small to explain the elevated concentration in this area found in the West Atlantic Geotraces observations (see bottom right in Fig. 8).

4. Discussion

4.1. Comparison with Gehlen et al. (2003)

Since our model is very similar to the model of Gehlen et al. (2003), a good agreement between our results and theirs is expected.

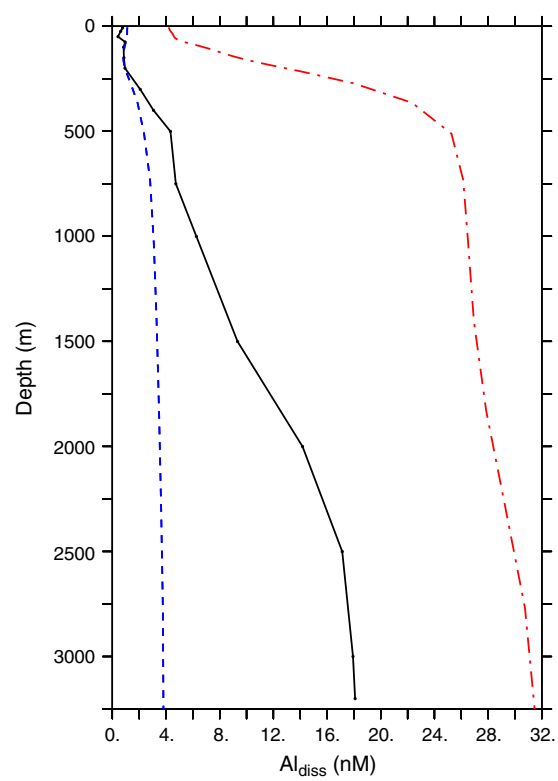

Fig. 15. [Al_{diss}] (nM) profile from a station in the eastern Arctic (ARKXXII/2): observations (black solid line), the reference simulation (blue dashed line), and sediment sensitivity simulation (red dash-dotted line), all at 213.6°E, 87.03°N.

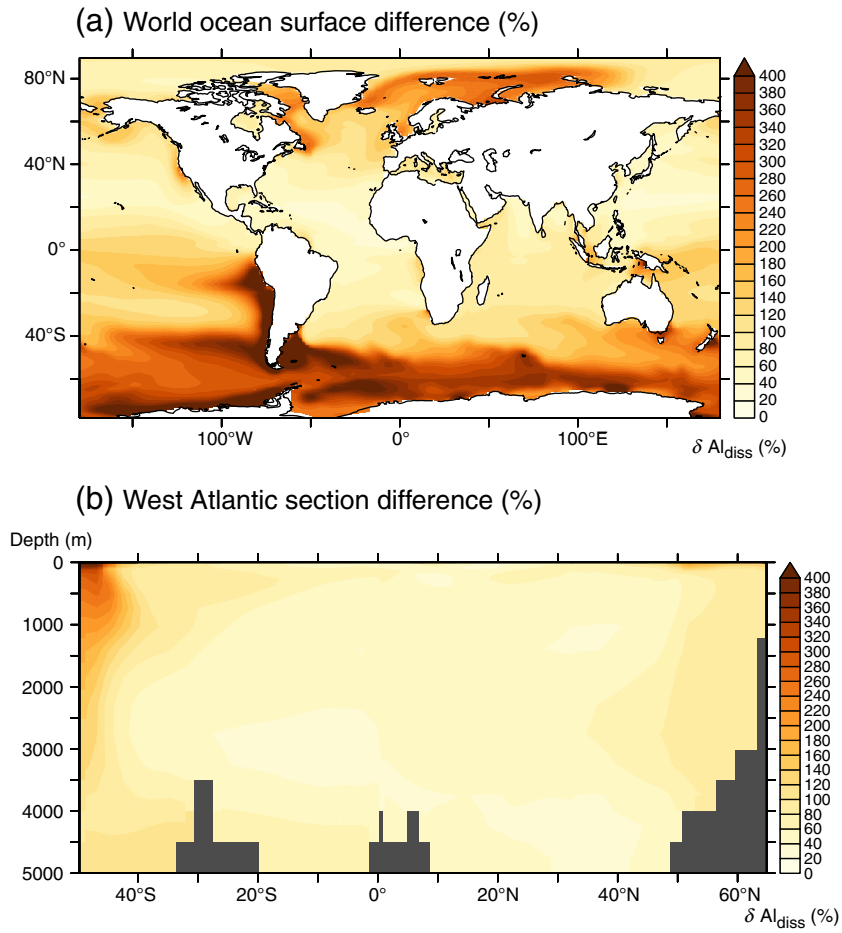

Fig. 16. The difference of the experiment with a decreased k_d relative to the reference experiment.

Even though several features in the two model results are the same, there are also noteworthy differences. These can arise because of differences in the ocean physics, the dust deposition field, as well as the biogeochemical model.

For the velocities the output of the NEMO model on the ORCA2 configuration is used in our model. On the other hand, in the model of Gehlen et al. (2003) a climatology from the Hamburg Large-Scale Geostrophic (LSG) OGCM is used (Maier-Reimer et al., 1993). The basic characteristics of the physics of the two models are the same, but a few features, like the mixed layer depth (MLD) and the Atlantic MOC, are significantly different. Even though LSG is a low resolution model, the depth of the meridional southward return flow of the Atlantic MOC is almost 3 km deep, which is realistic. On the other hand, in the OPA model (with the ORCA2 configuration) this return flow is much more shallow (a bit over 2 km deep), as shown in Fig. 9. A shallow return flow is typical for low resolution models (e.g. Dutay et al., 2002). Furthermore, the AABW in LSG goes to 15°N, while in our model it goes all the way to 40°N. Overall, the physics of the two models are comparable, but we should keep in mind that the overturning in the ORCA2 configuration of OPA is too shallow and AABW goes too far north, compared with the LSG model.

In both the work of Gehlen et al. (2003) and in our work, the highest concentration of Al_{diss} is found in the surface model layer (Fig. 5) in the Atlantic Ocean around 20°N. In both models the Al_{diss} concentration is low in the Southern Ocean and in the Pacific Ocean. However, there are distinct differences of [Al_{diss}] in the surface ocean in the models. Several features visible in the observations are better captured by the model of Gehlen et al. (2003), while other features are simulated better by our model. These differences are likely to be due to the different dust deposition fields used in the model of Gehlen et al. (2003) compared to the one we used.

In the eastern Atlantic Ocean around 20°N near the coast of Africa, Gehlen et al. (2003) simulate a Al_{diss} concentration of over 300 nM, or around 50 nM for a different dust deposition field. The concentrations in our model and the observations, however, are generally around 30 nM.

In and near the Indonesian Archipelago [Al_{diss}] ranges from 1 to 20 nM in both models, while the observations of Obata et al. (2007) and Slemons et al. (2010) are much more homogeneous, about 10 nM. This might be because the ocean currents in both models are not realistic because of a too low resolution of our model for this region. Possibly other effects in the real ocean play a role, like sedimentary input from the Indonesian Archipelago and east of Indonesia (see Fig. 2(b) for the relative importance).

The vertical meridional section in Fig. 8 through the West Atlantic Ocean shows a reasonable correspondence between the two models. The concentration at the surface is high in both models, it roughly decreases with depth in the Atlantic Ocean. In the Southern Ocean aluminium concentrations are low in the whole column, but especially in the surface (Fig. 8, very left). However, in our model between 10°S and 45°N there is a significant decrease of [Al_{diss}] with depth, which is not visible in the model results of Gehlen et al. (2003) where below 2 km north of the equator [Al_{diss}] is rather homogeneous in both dimensions along the cross-section. The model of Gehlen et al.

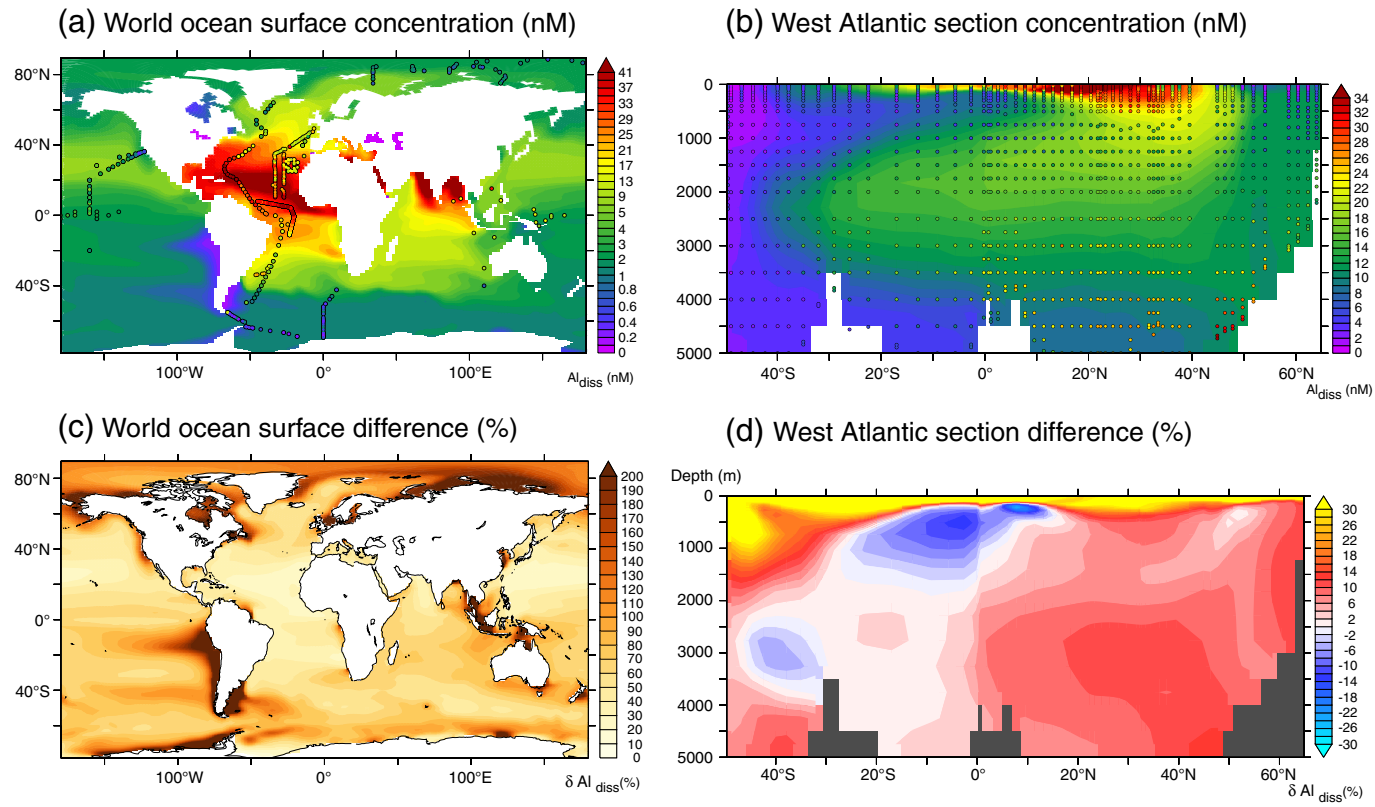

Fig. 17. [Al_{diss}] (nM) in the slow-equilibration experiment ($\kappa = 100$ year^{-1}) and the relative difference with the reference experiment ($\kappa = 10^4$ year^{-1}).

(2003) shows North Atlantic Deep Water (NADW) in the [Al_{diss}] Al_{diss} distribution, spreading southward at a depth of almost 3 km, as also shown by the observations (Fig. 8, but also Van Aken, in preparation). Our model also captures NADW, but this is at only 2 km depth, as explained before.

4.2. Advection versus scavenging

While Al is entering the ocean through the surface by dust deposition and leaving it at the bottom through burial, it is also transported by the currents. In this section we try to find out whether scavenging or advection is more important in setting the modelled Al concentration at different regions of the ocean.

In our model scavenging is reversible, which we base on a priori arguments (Anderson, 2006; Bacon and Anderson, 1982) and the general increase of [Al_{diss}] with depth in observations. Therefore it is unexpected that in the Atlantic Ocean a depth decreasing profile of Al_{diss} is simulated (see e.g. Fig. 17(b)).

One possible reason for this is that the $bSiO_2$ distribution is not realistic. However, the PISCES model with the Si cycle is used by several modelling studies (Arsouze et al., 2009; Aumont and Bopp, 2006; Dutay et al., 2009; Tagliabue et al., 2010) and has the same spatial patterns as known $bSiO_2$ export fields (e.g. Sarmiento and Gruber, 2006).

It should be emphasised that we only scavenge Al by biogenic silica. Of course $CaCO_3$ and POC might also scavenge in reality. Looking back to our comparison with the observations of Middag et al. (in preparation), we found that near Greenland [Al_{diss}] was overestimated by the model. This would be an example where the addition of other scavengers, especially $CaCO_3$ can help in decreasing the modelled [Al_{diss}] near Greenland, and also in the western South Atlantic Ocean between 30 and 40°S. Refer to e.g. Dittert et al. (2005), Sarmiento and Gruber (2006) for export of $bSiO_2$, $CaCO_3$ and POC; or Lam (2011) for concentrations.

The importance of scavenging is visible from several features in our model data. Firstly, Fig. 7 shows that on a global scale the pattern of [Al_{diss}] has roughly the same form at different depths, which is a result of reversible scavenging, i.e., at the surface where [$bSiO_2$] is high, Al is mainly adsorbed onto $bSiO_2$, while at depth Al is mostly desorbed from $bSiO_2$. Specifically, [Al_{diss}] is high in the Atlantic and Indian Oceans north of 30°S, and much lower in other regions of the ocean. Secondly, the fact that the concentration in the Pacific Ocean is low at all depths, is because Al_{diss} is removed by scavenging before it reaches the Pacific Ocean. These are just a few of the features in the Al_{diss} distribution that suggest that on a large scale scavenging is more important than advection.

However, the observations and the model show that advective transport by ocean currents is important as well. For instance, Fig. 2(a) shows that large quantities of dust are deposited just west of the Sahara. However, large concentrations of Al_{diss} are not only visible directly below the dust deposition site, but even higher concentrations are found further to the west (Fig. 5). Large amounts of dissolved Al must be advected from the dust deposition site toward Central America. Hereafter it seems to be advected northward until Iceland, where [Al_{diss}] is high despite very little dust deposition. Deeper in the North Atlantic Ocean the original dust signal decreases, and at 2 km depth in the model (or 3 km depth in the observations) Al_{diss} is transported into the southern hemisphere by the NADW. This southward transport can be seen clearly in Fig. 8, but no further than 40°S. South of this latitude the Al_{diss} concentration is low.

These examples indicate that also advection plays an important role in the redistribution of Al.

4.2.1. Timescales

While the analysis of [Al_{diss}] distributions points to the combined importance of scavenging and advection in setting its overall pattern, it does not allow to quantify their relative importance. In order to

assess the relevance of these different processes, associated timescales are defined based on our model equations.

A priori the relative relevance of scavenging can partly be derived from the model equations. Substituting Eq. (3) into Eq. (2) yields:

$$\frac{d}{dt}[\mathrm{Al}_{ads}] = \kappa \cdot \left([A^{eq}_{ads}] - [\mathrm{Al}_{ads}]\right) = \frac{1}{\tau_{ads}}[\mathrm{Al}_{diss}] - \frac{1}{\tau_{eq}}[\mathrm{Al}_{ads}], \tag{8}$$

where $\tau_{ads} = 1/(\kappa k_d[bSiO_2])$, is the typical adsorption timescale. This is the typical time necessary for Al to transform from Al_{diss} to Al_{ads} (or vice versa). This process depends on the amount of available $bSiO_2$ and the amount of Al_{diss} which can adsorb onto $bSiO_2$, giving the actual rate of conversion between Al_{diss} and Al_{ads}. The addition of Al_{ads} is equal to the removal of Al_{diss}, so τ_{ads} is either the time necessary to add Al_{ads}, or the time to remove Al_{diss}. The second timescale in Eq. (8), $\tau_{\mathrm{eq}} = 1/\kappa$, is the time it takes for Al_{ads} to equilibrate to Al^{eq}_{ads}. This process provides a stabilising feedback on the growth of $[\mathrm{Al}_{ads}]$ (or decrease of $[\mathrm{Al}_{diss}]$).

Scavenging is the process of adsorption and sinking, so we need to know how fast particles sink. This is used together with the adsorption timescale to define a scavenging timescale. Since the surface ocean is analysed, the typical sinking speed might be defined as sinking through the first 10 m, the thickness of the upper model gridbox. However, after exporting Al_{ads} out of a gridbox by sinking, the particles sink through the mixed layer (which is generally thicker than 10 m). During sinking, the particles will partly be mixed back into the upper gridbox. Therefore to speak of a removal, it is a necessary condition for Al to sink out of (at least) the mixed layer. In our model, the sinking velocity of $bSiO_2$ and Al_{ads} is defined to be constant in the mixed layer, namely $w_s = 30$ m/day. Now it is easy to define the typical sinking timescale: $\tau_{\mathrm{sink}} = D_{\mathrm{ML}}/w_s$, where D_{ML} is the mixed layer depth. The scavenging timescale can be defined as the maximum of the adsorption and the sinking timescales:

$$\tau_{scav} = \max(\tau_{ads}, \tau_{sink}). \tag{9}$$

This signifies how fast Al is exported from the mixed layer. Except for a few places where the mixed layer is very deep, like the centre of the Labrador Sea, the time it takes to sink out of the mixed layer is generally very small compared to the time it takes the Al to adsorb onto a particle ($\tau_{\mathrm{sink}} \ll \tau_{\mathrm{ads}}$) and thus almost everywhere $\tau_{\mathrm{scav}} = \tau_{\mathrm{ads}}$.

A typical advection timescale is defined as follows:

$$\tau_{adv} = \min\left(\frac{L}{V}, \frac{D_{\mathrm{ML}}}{W}\right). \tag{10}$$

Here L is the typical length scale, defined as the horizontal diameter of a gridbox, and V is the horizontal speed. Since the vertical velocity component is very small ($W \ll (D_{\mathrm{ML}}/L)U$), at most locations only the horizontal components need to be considered, but for correctness the vertical advection W is included in the calculation as well. The meaning of this timescale is that within a time τ_{adv} Al_{diss} (or any other non-buoyant tracer) is advected out of a gridbox (if it is not scavenged before).

The residence time can be defined as the minimum of the scavenging and the advection timescales $\tau_{\mathrm{res}} = \min(\tau_{scav}, \tau_{adv})$. It is the typical time that Al_{diss} stays within a volume box of horizontal grid resolution (about $2^\circ \times 2^\circ$) times D_{ML}. This quantity is presented in Fig. 18.

The oligotrophic gyres in the Atlantic, Pacific and Indian Oceans are clearly visible. In the centre of these gyres it takes much longer than 1 year before Al is exported out of a volume box, either by advection or by scavenging. The modelled Al_{diss} distribution of Fig. 5 shows in the Atlantic Ocean the largest values between 10 and 30°N. This can be partly explained by the large dust input between 5 and 20°N, where Al_{diss} is removed relatively fast by advection but dust input keeps $[\mathrm{Al}_{diss}]$ large, and partly by the large residence time between 20 and 30°N, where there is no large dust input but Al_{diss} simply stays there for a long time, since there is no $bSiO_2$ present for scavenging and advection is very small. A similar argument can be given for the high $[\mathrm{Al}_{diss}]$ near the North Pacific gyre.

If we want to know which of the timescales are more important, a relative relation between τ_{scav} and τ_{adv} must be defined. The number for relative importance of scavenging versus advection for Al export is the following:

$$\Upsilon = \frac{\tau_{\mathrm{adv}}}{\tau_{\mathrm{scav}}}. \tag{11}$$

The logarithm of this quantity is plotted in Fig. 19. In regions where $\Upsilon \gg 1$, like north of 40°N in the Atlantic and Pacific Oceans and in the south of the Southern Ocean, scavenging is more important than advection. On large scales the large Υ regions coincide very well with the large $bSiO_2$ regions (Fig. 6). Looking more in detail, we can see that Υ is less homogeneous than $[bSiO_2]$. For instance, in the Drake Passage and in the Pacific sector of the Southern Ocean at 150°W the timescale fraction is smaller than one would expect based on the $bSiO_2$ distribution. This is because of the strong velocity of the Antarctic Circumpolar Current (see Fig. 1).

In regions where $\Upsilon \ll 1$, in the low latitudes, advection is more important than scavenging. One can say that if $\Upsilon \ll 1$, $[\mathrm{Al}_{diss}]$ is advection driven, while for $\Upsilon \gg 1$, $[\mathrm{Al}_{diss}]$ is scavenging driven. In the high Υ regions a one-dimensional model would be a reasonable approximation, provided that there is sufficient Al input to keep $[\mathrm{Al}_{diss}]$ in steady state.

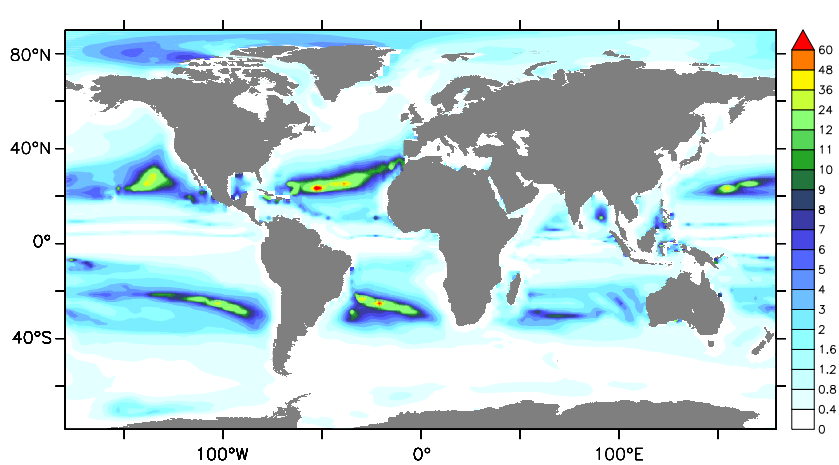

Fig. 18. Mean local residence time (in months) of dissolved Al in the surface mixed layer based on scavenging and advection processes.

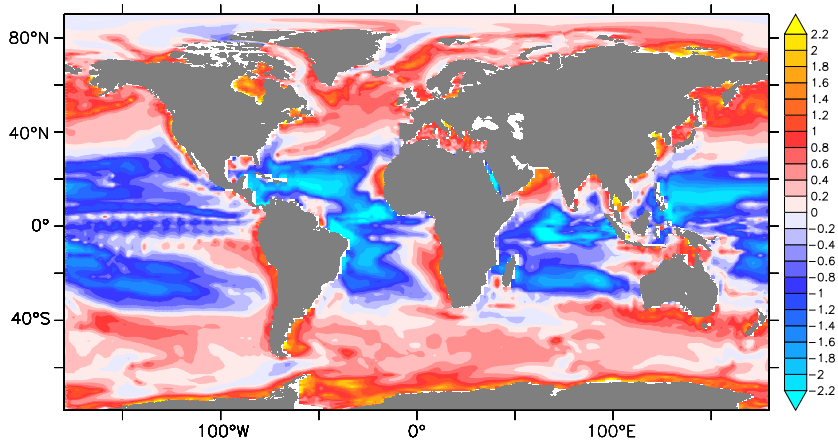

Fig. 19. Log $_{10}(\Upsilon)$, when $\kappa = 10^4$ year^{-1} and $k_d = 4 \cdot 10^6$ l/kg. For the advection time τ_{adv} the definition of Eq. (10) is used, and the scavenging time τ_{scav} is the maximum of τ_{ads} and τ_{sink}.

One region where this should perfectly work is the Mediterranean – there Υ is very large and the dust flux is high. Several other regions like the northern seas, near Antarctica and some other coastal areas would also be good candidates for a one-dimensional model. Other regions of the ocean cannot be well described by a one-dimensional model. Specifically the Arctic Ocean would not be a good candidate. Even though it is a semi-closed basin, internal circulation has an effect of the same order as scavenging. These arguments must be taken into consideration when using one-dimensional models.

4.3. Ocean sediments source

Including margin sediment input of Al results in overestimated values for [Al_{diss}] compared to the observations in the Arctic Ocean. Potential reasons for this will now be discussed. As described in Section 2.1.3 the Al flux is proportional to the Fe flux which depends on the degree of oxygenation of the sediments. This is probably not a reasonable assumption, since generally Al does not flow out of undisturbed sediments, but enters the water column through resuspension of the sediments (e.g. Mackin, 1986; Van Beusekom et al., 1997). Since there is not enough data on resuspension rates, we chose this simplistic parametrisation for our sensitivity experiment. A priori we therefore have no reason to expect an improvement in the model. The sensitivity experiment can only be used to get an idea of the first-order effects of an ocean sediment source of Al, henceforth referred to as "sediment input". Since the sediment input in the Arctic Ocean is treated in the same way as the rest of the ocean, it is surprising that [Al_{diss}] gets much too high (Fig. 14), certainly when considering the improvement in the West Atlantic as described below. There is a lack of knowledge of boundary exchange processes (e.g. Arsouze et al., 2009), which keeps open the possibility that the large sediment source from the margins is compensated by boundary exchange processes. In our model only $bSiO_2$ was used as a scavenger, while near the margins, other scavengers like POC and $CaCO_3$ might play an important role. Also scavengers not present in the PISCES model, like clay minerals (Walker et al., 1988) might be important for reducing [Al_{diss}]. The possibility of this boundary scavenging (Arsouze et al., 2009; Bacon et al., 1988) is convincingly shown to be present in observations (e.g. Brown et al., 2010). Since most of the data used here is from the open ocean and not from coastal areas, and our model is too coarse for an analysis of the coastal aluminium concentrations, it is not possible to make a good a priori estimate of the amount of sediment input needed for a better simulation. Since dust input and internal processes contain parameters which are, just like sediment input, not completely constrained, a change in sediment input could result in a simulation which predicts the open ocean aluminium concentration better, but does a bad job in other areas. Nevertheless, consistent with work by Middag et al. (2011), Moran and Moore (1991), and Moran et al. (1992), there are clearly some areas where sediment supply of Al_{diss} appears important and a better understanding of the processes governing its supply is needed.

4.4. Internal coefficients

For the experiments where we changed two internal parameters (k_d and κ) the simulations can now be analysed in a more sophisticated manner by using the above timescale approach. As can be seen from the black dash-dotted line in Fig. 20, the effect of a halved partition coefficient k_d on the whole ocean is an almost doubling of the total Al budget. According to Eq. (3) indeed a halved k_d means half as much [Al_{ads}^{eq}]. In all experiments equilibration is very fast, except the one where κ is decreased significantly. Because of the fast equilibration, with halved k_d, export will be half as fast. In a steady state, this would result in a doubled Al_{diss} content, if $bSiO_2$ would be distributed homogeneously. Since it is not, this does not hold for our model. At the dust deposition site in the Atlantic Ocean, Fig. 16(a) shows an increase of [Al_{diss}] of less than 100% in the Atlantic Ocean near the dust deposition site. Because of the reduced k_d more Al_{diss} can be transported northward. When it reaches large [$bSiO_2$], it is scavenged with twice the speed compared to the reference simulation. Since this extra Al_{diss} was able to reach the high [$bSiO_2$] site, the effect of the reduced k_d is dampened and therefore the ocean Al budget is less than doubled. Since the relative effect of advection compared to scavenging can be different in this simulation, Υ should be analysed. This timescale ratio is proportional to k_d and [$bSiO_2$] (see Eq. (11)). Halving k_d results in only a small change in importance of scavenging relative to advection (compare Fig. 19 with Fig. 21(a)). A decrease in the first-order rate constant κ means that equilibration goes slower (Eq. (2)). If dust is dissolved in the surface ocean, its conversion to Al_{ads} is slower, so that Al_{diss} is scavenged slower. Because of the resulting higher [Al_{diss}], more aluminium is transported northward by the North Atlantic Current. Fig. 6 shows the biogenic silica ($bSiO_2$) concentration according to the model at the surface. In the Atlantic Ocean are high concentrations of $bSiO_2$ north of 40°N. The dissolved Al, which arrives in this area, is scavenged by this high [$bSiO_2$]. This results in high concentrations at all depths around 40°N. However, because of slow equilibration, Al_{diss} can go further north before it is actually scavenged. This is the reason why a significant increase in [Al_{diss}] is visible around 60°N at all depths, and also further south at a depth around

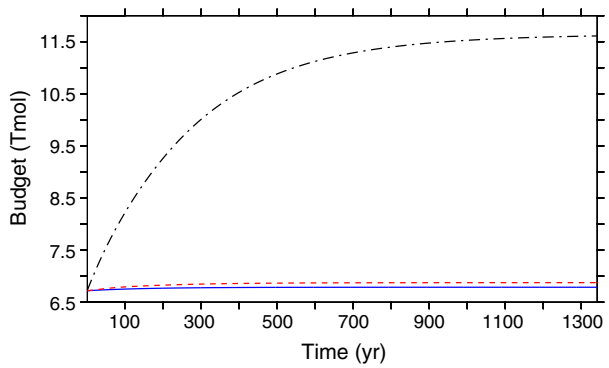

Fig. 20. Total Al budget (Tmol) in the world ocean after a partial spin-up of 600 years of the reference simulation. From this point the reference simulation together with the sensitivity experiments is run for another 1300 years or more. The blue solid line is the budget of the reference simulation, the red dashed line of the slow-equilibration simulation and the black dash-dotted line of the simulation with a decreased partition coefficient.

2 km because this extra Al is advected southward via the MOC (Fig. 17(d)). Also desorption goes slower, which means that Al_{diss} that is adsorbed at the surface around 40°N, will desorb slowly while sinking, such that compared to the reference simulation a relatively large quantity of Al_{diss} will appear in the deep Atlantic Ocean. This can be seen in the lower right of Fig. 17(d).

According to Fig. 17(d) there is a decrease of $[Al_{diss}]$ at low latitudes around 500 m and 1 km depth. Less dissolved Al from dust in the surface ocean is scavenged and therefore less adsorbed aluminium is present in the deeper regions to desorb at depth. So in the deep ocean there are regions of increased $[Al_{diss}]$ and regions of decreased $[Al_{diss}]$.

If a lot of particulate aluminium sinks where there is almost no biogenic silica, it will desorb and the resulting Al_{diss} will stay there. According to the equations, with a very large κ this will happen instantaneously and the dissolved aluminium will stay there indefinitely (in the limit of zero biogenic silica and zero advection), i.e., $\tau_{res} = \infty$. This really means, as discussed in Section 4.2.1, that in that case advection is much more important than scavenging. If κ is decreased, the particulate aluminium has enough time to fall out of this low biogenic silica domain before it desorbs.

In Fig. 21(b) the logarithm of the relative importance of scavenging, Υ, is plotted for the slow-equilibration experiment. It shows that everywhere advection is more important than scavenging. As a consequence, the Al_{diss} distribution obtained with a low κ is more homogeneous than in the reference experiment. As can be seen from the dashed red line in Fig. 20, the relative increase of the Al budget is very small. The only strong increase is in the surface ocean. In the rest of the ocean, $[Al_{diss}]$ is just homogenised.

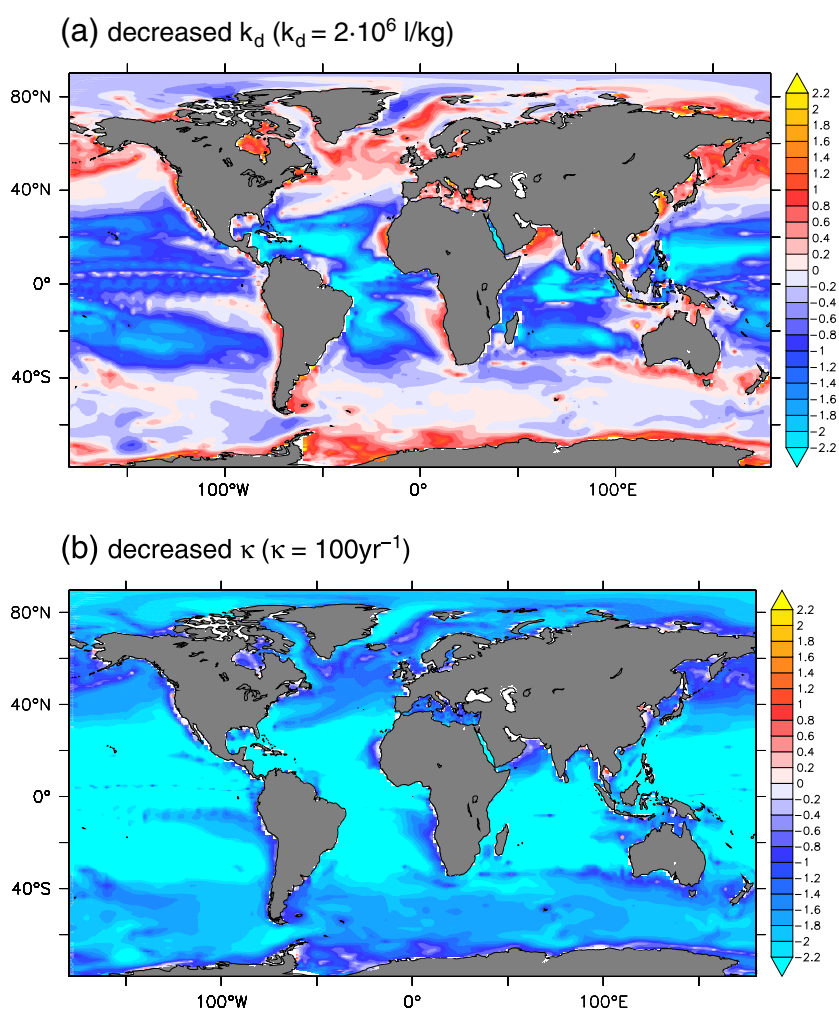

Fig. 21. Log $_{10}(\Upsilon)$, for different adsorption parameters. For the advection time τ_{adv} the definition of Eq. (10) is used, and the scavenging time τ_{scav} is the maximum of τ_{ads} and τ_{sink}.

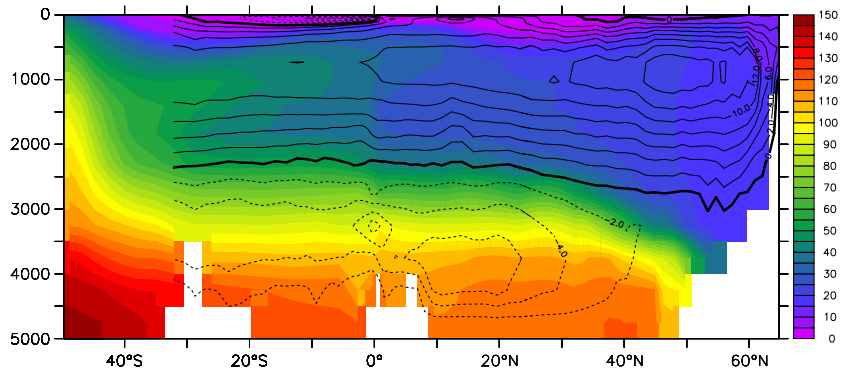

Fig. 22. The quantity in the coloured area is [Si_{diss}] (μM) at the Geotraces West Atlantic cruise section. The contours represent the Atlantic Overturning Stream Function (Sv).

4.5. Al versus Si in the MOC

Our modelling results in the Atlantic Ocean show that at around 2 km depth [Al_{diss}] decreases from north to south, while the concentration of dissolved silicon (Si_{diss}) increases, all the way into the Pacific Ocean, both following the Meridional Overturning Circulation (MOC). This is shown in Figs. 22 and 9, representing the concentrations of Si_{diss} and Al_{diss} respectively in the West Atlantic Ocean. On top of these figures a contour of the Atlantic Overturning Stream Function (OSF) in Sv (1 Sv = 10^6 m^3s^{-1}) of the physical forcing is plotted.

The patterns for both [Al_{diss}] and [Si_{diss}] are in first order easily interpreted by looking at the source of the tracer and the general currents in the Atlantic Ocean. The source of Al_{diss} is dust dissolution in the surface of the central Atlantic Ocean. It is transported northward by the Gulf Stream and the North Atlantic Current. Before the Al_{diss} reaches locations where NADW is formed, it is scavenged by biogenic silica from 40°N northward (Fig. 6) and based on our timescale analysis (Fig. 19) possibly already near 30°N. Because of remineralisation [Al_{diss}] increases in the NADW. This is consistent with the fact that in the model Al_{diss} does not nicely follow the Atlantic MOC in the very north of the Atlantic Ocean, but rather tends to sink into the NADW indeed near 30°N. After this the Al_{diss} is taken along with the NADW, reaching 40°S at around 2 km depth. To complete the picture of the modelled Al_{diss} distribution, low [Al_{diss}] SAAMW/AAIW enters just below the surface of the Atlantic Ocean from the Southern Ocean, and low [Al_{diss}] AABW into the Atlantic Ocean below 4 km depth.

The source of Si_{diss} is the large amount of diatoms that sink and remineralise south of 50°S, after which it is advected as AABW as clearly shown in Fig. 4. Other features visible are the SAAMW/AAIW moving below the surface of the Atlantic Ocean and low [Si_{diss}] NADW diluting the dissolved Si concentration in the Atlantic Ocean (Fig. 22).

The pattern of [Si_{diss}] is similar to the observations described by Middag et al. (in preparation). The main difference is that the model overestimates [Si_{diss}] in the deep North Atlantic Ocean, and is a little bit too low in the deep South Atlantic Ocean. This is consistent with the overestimated AABW inflow in the model velocity field.

According to observations, in the lower cell of the Atlantic MOC, the OSF reaches a maximum of 1 or 2 Sv, while according to our physical model forcing its maximum is about 6 Sv. Furthermore, the AABW does not go as far north as in our model. Because of this the transport of any tracer following the pathway of AABW will be too large. Therefore [Si_{diss}] is overestimated in the deep North Atlantic Ocean. Coming back to the discussion in Section 3.1.1, because of the same reasons [Al_{diss}] is too quickly diluted in the deep North Atlantic Ocean.

The underestimation of [Al_{diss}] in the deep North Atlantic Ocean is more significant than the overestimation of [Si_{diss}] in this same area. This suggests there might be another process playing a role. A likely candidate is an adjusted depth-depending sinking velocity of $bSiO_2$ and Al_{ads} which is depth-increasing in our current model. Recent observations (McDonnell, 2011; McDonnell and Buesseler, 2010) suggest that sinking speed is not strictly depth-increasing, but other functions with depth should be considered. Also more sophisticated aggregation methods should be studied, as for instance done in models by Burd and Jackson (2009), Gehlen et al. (2006), and Kriest and Evans (1999), even though none of these specific efforts give results consistent with the study by McDonnell and Buesseler (2010). Another possibility is that the model needs sediment sources more sophisticated than in our sensitivity experiment, as also shown by observations by Middag et al. (in preparation) and Moran et al. (1992) (and references therein).

5. Conclusions and outlook

The objective of this study is to come to a better understanding of the behaviour of Al, by means of simulating the Al_{diss} distribution in the ocean with a reversible scavenging and general circulation model, and comparing it to observations. In turn, these results can be used for further developing this model to simulate the Al distribution more precisely. A more realistic simulation could then be used for constraining dust deposition fields to more precisely derive nutrient input rates. It can also be used to study further the influence of sediments on the water column [Al_{diss}], e.g. by means of coupling the ocean model to a sediment model.

The biogeochemical model PISCES is run off-line, forced by a climatological velocity field with a temporal resolution of 5 days and a monthly dust deposition field. In one of the sensitivity experiments a margin sediment source is included, which has not been done before for Al.

We are able to simulate the main features of the global Al_{diss} distribution in accordance with available observations. Specifically we are able to simulate reasonably well the distribution in the West Atlantic compared to observations from the West Atlantic Geotraces cruises.

Since our results are close to observations, we can assume that the Al distribution is indeed mainly controlled by advection and reversible scavenging, with $bSiO_2$ as the main scavenger. It is possible to improve specific features of the distribution by changing certain parameters of the scavenging process, or adjusting the Al sources. Increasing dust Al dissolution results in an overall aluminium increase proportional to the increased dust factor everywhere in the ocean. Adding dissolution in the water column gives higher concentrations, especially near dust deposition sites around one or two km depth. Decreasing the partition coefficient k_d results in a higher concentration of Al_{diss} everywhere in the ocean. Especially the relative increase in the Al_{diss} concentration in the Southern Ocean is large. This parameter highlights the importance of the influence of spatial variability in biogenic silica on [Al_{diss}], since k_d signifies the amount of Al_{diss} which can adsorb onto $bSiO_2$. When

including sediments as an input to Al_{diss}, elevated concentrations are seen, especially near the margins, as expected. [Al_{diss}] is strongly elevated in the Arctic Ocean, which is not reconcilable with the observations, and is possibly due to the lack of oceanic-margin scavengers in the model. The model should be modified such that a realistically constrained ocean margin source of Al_{diss} is present.

By means of a timescale analysis based on our model equations, we have shown that the importance of scavenging versus advection is highly location dependent. The local residence time is strongly space dependent as well. Especially latitudinal gradients are large. This residence time varies between less than a week at high [$bSiO_2$] and strong advection, to many years in the oligotrophic gyres.

Even though the most relevant features of the Al_{diss} distribution are captured, some fine tuning of the key parameters is necessary. There is clearly a localised source missing in the West Atlantic between 45 and 50°N near the sediment. As already hypothesised by Moran and Moore (1991), resuspension of nepheloid layers along the western boundary of the North Atlantic Ocean is a source of Al_{diss}. A more detailed analysis of the locally elevated [Al_{diss}] in the West Atlantic near 45°N is in progress (Middag et al., in preparation).

Another location of interest is the Arctic Ocean, where we could not simulate the observations. This is possibly because we miss a sediment source, or an important process is missing in the model, namely the biological incorporation of Al into the diatom's frustules (Caschetto and Wollast, 1979; Gehlen et al., 2002). If this process would be implemented in the model, dissolved Al could be taken up by diatoms in the surface ocean and released in the deep ocean when the biogenic silica is remineralised together with the incorporated Al, yielding a strong Al:Si correlation as present in the observations (Middag et al., 2009).

Good progress is made in simulating the distribution of dissolved aluminium in the world ocean, and our approach confirms that dust deposition is the main source of aluminium and reversible scavenging is the main process in removing it. However, significant improvement might be possible by (1) developing a more sophisticated model for ocean sediment source of Al, (2) adding diatom Al incorporation, and (3) fine tuning the free parameters and constraining them by means of field studies and laboratory experiments to better understand the role for these processes.

Acknowledgements

The authors are grateful to those who have been proved useful in discussion, among which Jack Middelburg, Laurent Bopp, Micha Rijkenberg and Wilco Hazeleger. Furthermore, we want to thank our colleagues from the IMAU institute for their critical and useful feedback to the model configuration and output. We also want to thank the people who kindly provided their datasets that are mentioned in this paper. Christoph Heinze kindly dug up the model data from Gehlen et al. (2003) and made it available to us.

The comments of two anonymous reviewers significantly improved this manuscript.

The authors wish to acknowledge use of the Ferret free software program for analysis and graphics in this paper. Ferret is a product of NOAA's Pacific Marine Environmental Laboratory (http://ferret.pmel.noaa.gov/Ferret/). Other noteworthy free software used is the *GNU Operating System* and *Climate Data Operators* (cdo).

This research is funded by the Netherlands Organisation for Scientific Research (NWO), grant Nr. 839.08.414.

Appendix A. Supplementary data

Supplementary data to this article can be found online at http://dx.doi.org/10.1016/j.jmarsys.2012.05.005.

References

van Aken, H., 2011. GEOTRACES, the hydrography of the Western Atlantic Ocean.
Anderson, R., 2006. Chemical tracers of particle transport. In: Elderfield, H. (Ed.), The Oceans and Marine Geochemistry, Vol. 6. Elsevier, pp. 247–274 (chapter 6.09).
Arsouze, T., Dutay, J.-C., Lacan, F., Jeandel, C., 2009. Reconstructing the Nd oceanic cycle using a coupled dynamical–biogeochemical model. Biogeosciences 2829–2846 http://dx.doi.org/10.5194/bg-6-2829-2009.
Aumont, O., Bopp, L., 2006. Globalizing results from ocean in situ iron fertilization studies. Global Biogeochem. Cycles http://dx.doi.org/10.1029/2005GB002591.
Aumont, O., Bopp, L., Schulz, M., 2008. What does temporal variability in aeolian dust deposition contribute to sea-surface iron and chlorophyll distributions? Geophys. Res. Lett. L07607- http://dx.doi.org/10.1029/2007GL031131.
de Baar, H., Boyd, P., Coale, K., Landry, M., Tsuda, A., Assmy, P., Bakker, D., Bozec, Y., Barber, R., Brzezinski, M., et al., 2005. Synthesis of iron fertilization experiments: from the iron age in the age of enlightenment. J. Geophys. Res. C09S16 http://dx.doi.org/10.1029/2004JC002601.
Bacon, M., Anderson, R., 1982. Distribution of thorium isotopes between dissolved and particulate forms in the deep sea. J. Geophys. Res. 2045–2056 http://dx.doi.org/10.1029/JC087iC03p02045.
Bacon, M., Roether, W., Elderfield, H., 1988. Tracers of chemical scavenging in the ocean: boundary effects and large-scale chemical fractionation [and discussion]. Philos. Trans. R. Soc. Lond. A 147 http://dx.doi.org/10.1098/rsta.1988.0048.
Baker, A., Jickells, T., Witt, M., Linge, K., 2006. Trends in the solubility of iron, aluminium, manganese and phosphorus in aerosol collected over the Atlantic Ocean. Mar. Chem. 43–58 http://dx.doi.org/10.1016/j.marchem.2005.06.004.
van Bennekom, A., Buma, A., Nolting, R., 1991. Dissolved aluminium in the weddell-scotia confluence and effect of al on the dissolution kinetics of biogenic silica. Mar. Chem. 423–434 http://dx.doi.org/10.1016/S0304-4203(09)90034-2.
van Beusekom, J., van Bennekom, A., Tréguer, P., Morvan, J., 1997. Aluminium and silicic acid in water and sediments of the Enderby and Crozet basins. Deep-Sea Res. II Top. Stud. Oceanogr. 44, 987–1003 http://dx.doi.org/10.1016/S0967-0645(96)00105-1.
Boyd, P., Jickells, T., Law, C., Blain, S., Boyle, E., Buesseler, K., Coale, K., Cullen, J., De Baar, H., Follows, M., et al., 2007. Mesoscale iron enrichment experiments 1993–2005: synthesis and future directions. Science 315, 612–617 http://dx.doi.org/10.1126/science.1131669.
Broecker, W., Peng, T.-H., 1982. Tracers in the Sea. Eldigio Press.
Brown, M., Lippiatt, S., Bruland, K., 2010. Dissolved aluminum, particulate aluminum, and silicic acid in northern Gulf of Alaska coastal waters: glacial/riverine inputs and extreme reactivity. Mar. Chem. 160–175 http://dx.doi.org/10.1016/j.marchem.2010.04.002.
Bruland, K., Lohan, M., 2006. Controls of trace metals in seawater. In: Elderfield, H. (Ed.), The Oceans and Marine Geochemistry, Vol. 6. Elsevier, pp. 23–47 (chapter 6.02).
Burd, A., Jackson, G., 2009. Particle aggregation. Ann. Rev. Mar. Sci. 65–90 http://dx.doi.org/10.1146/annurev.marine.010908.163904.
Caschetto, S., Wollast, R., 1979. Vertical distribution of dissolved aluminium in the Mediterranean Sea. Mar. Chem. 141–155 http://dx.doi.org/10.1016/0304-4203(79)90006-9.
Chou, L., Wollast, R., 1997. Biogeochemical behavior and mass balance of dissolved aluminum in the western Mediterranean Sea. Deep-Sea Res. II Top. Stud. Oceanogr. 44, 741–768 http://dx.doi.org/10.1016/S0967-0645(96)00092-6.
Dittert, N., Corrin, L., Bakker, D., Bendtsen, J., Gehlen, M., Heinze, C., Maier-Reimer, E., Michalopoulos, P., Soetaert, K., Tol, R., 2005. Integrated Data Sets of the EU FP5 Research Project: ORFOIS: Origin and Fate of Biogenic Particle Fluxes in the Ocean and Their Interactions with Atmospheric CO2 Concentrations as Well as the Marine Sediment. : WDC-MARE Reports 0002, vol 1. Alfred Wegener Institute for Polar and Marine Research.
Dixit, S., Cappellen, P.V., 2002. Surface chemistry and reactivity of biogenic silica. Geochim. Cosmochim. Acta 2559–2568 http://dx.doi.org/10.1016/S0016-7037(02)00854-2.
Dixit, S., van Cappellen, P., van Bennekom, A., 2001. Processes controlling solubility of biogenic silica and pore water build-up of silicic acid in marine sediments. Mar. Chem. 333–352 http://dx.doi.org/10.1016/S0304-4203(00)00118-3.
Dutay, J., Bullister, J., Doney, S., Orr, J., Najjar, R., Caldeira, K., Campin, J., Drange, H., Follows, M., Gao, Y., et al., 2002. Evaluation of ocean model ventilation with cfc-11: comparison of 13 global ocean models. Ocean Modell. 89–120 http://dx.doi.org/10.1016/S1463-5003(01)00013-0.
Dutay, J., Lacan, F., Roy-Barman, M., Bopp, L., 2009. Influence of particle size and type on 231Pa and 230Th simulation with a global coupled biogeochemical-ocean general circulation model: a first approach. Geochem. Geophys. Geosyst. Q01011 http://dx.doi.org/10.1029/2008GC002291.
Emerson, S., Hedges, J., 2006. Sediment diagenesis and benthic flux. In: Elderfield, H. (Ed.), The Oceans and Marine Geochemistry, vol. 6. Elsevier, pp. 293–319 (chapter 6.11).
Ethé, C., Aumont, O., Foujols, M.-A., Lévy, M., 2006. NEMO reference manual, tracer component: NEMO-TOP. Preliminary version. Note du Pole de Modélisation. Institut Pierre-Simon Laplace.
Filella, M., 2007. Colloidal properties of submicron particles in natural waters. In: Wilkinson, K., Leas, J. (Eds.), Environmental Colloids and Particles: Behaviour, Separation and Characterisation, vol. 10. John Wiley & Sons, Ltd, pp. 17–94 (chapter 2).
Gary, S.F., Lozier, M.S., Böning, C.W., Biastoch, A., 2011. Deciphering the pathways for the deep limb of the Meridional Overturning Circulation. Deep-Sea Res. II Top. Stud. Oceanogr. 58, 1781–1797 http://dx.doi.org/10.1016/j.dsr2.2010.10.059.
Gehlen, M., Beck, L., Calas, G., Flank, A., Bennekom, A.V., Beusekom, J.V., 2002. Unraveling the atomic structure of biogenic silica: evidence of the structural association of Al and Si in diatom frustules. Geochim. Cosmochim. Acta 1601–1609 http://dx.doi.org/10.1016/S0016-7037(01)00877-8.

Gehlen, M., Heinze, C., Maier-Reimer, E., et al., 2003. Coupled Al-Si geochemistry in an ocean general circulation model: a tool for the validation of oceanic dust deposition fields? Global Biogeochem. Cycles 1028 http://dx.doi.org/10.1029/2001GB001549.
Gehlen, M., Bopp, L., Emprin, N., Aumont, O., Heinze, C., Ragueneau, O., 2006. Reconciling surface ocean productivity, export fluxes and sediment composition in a global biogeochemical ocean model. Biogeosciences 521–537.
Gehlen, M., Gangstø, R., Schneider, B., Bopp, L., Aumont, O., Ethe, C., 2007. The fate of pelagic CaCO3 production in a high CO2 ocean: a model study. Biogeosciences 505–519.
Goldberg, E., 1954. Marine geochemistry 1. Chemical scavengers of the sea. J. Geol. 249–265.
Guerzoni, S., Molinaroli, E., Chester, R., 1997. Saharan dust inputs to the western Mediterranean Sea: depositional patterns, geochemistry and sedimentological implications. Deep-Sea Res. II Top. Stud. Oceanogr. 44, 631–654.
Han, Q. (2010). Crustal Tracers in the Atmosphere and Ocean: Relating their Concentrations, Fluxes, and Ages. Ph.D. thesis University of California, Irvine.
Han, Q., Moore, J., Zender, C., Hydes, D., 2008. Constraining oceanic dust deposition using surface ocean dissolved Al. Global Biogeochem. Cycles http://dx.doi.org/10.1029/2007GB002975.
Hydes, D., Statham, P., Burton, J., 1986. A vertical profile of dissolved trace metals (Al, Cd, Cu, Mn, Ni) over the median valley of the mid Atlantic ridge, 43Å°N: implications for hydrothermal activity. Sci. Total. Environ. 133–145 http://dx.doi.org/10.1016/0048-9697(86)90236-6.
Hydes, D., de Lange, G., de Baar, H., 1988. Dissolved aluminium in the Mediterranean. Geochim. Cosmochim. Acta 2107–2114 http://dx.doi.org/10.1016/0016-7037(88)90190-1.
Jickells, T., 1995. Atmospheric inputs of metals and nutrients to the oceans: their magnitude and effects. Mar. Chem. 199–214.
Jickells, T., Church, T., Veron, A., Arimoto, R., 1994. Atmospheric inputs of manganese and aluminium to the Sargasso Sea and their relation to surface water concentrations. Mar. Chem. 283–292.
Jickells, T., An, Z., Andersen, K., Baker, A., Bergametti, G., Brooks, N., Cao, J., Boyd, P., Duce, R., Hunter, K., et al., 2005. Global iron connections between desert dust, ocean biogeochemistry, and climate. Science 308, 67 http://dx.doi.org/10.1126/science.1105959.
Kramer, J., Laan, P., Sarthou, G., Timmermans, K., De Baar, H., 2004. Distribution of dissolved aluminium in the high atmospheric input region of the subtropical waters of the North Atlantic Ocean. Mar. Chem. 85–101 http://dx.doi.org/10.1016/j.marchem.2004.03.009.
Kremling, K., 1985. The distribution of cadmium, copper, nickel, manganese, and aluminium in surface waters of the open Atlantic and European shelf area. Deep Sea Res. Part A 32, 531–555 http://dx.doi.org/10.1016/0198-0149(85)90043-3.
Kriest, I., Evans, G., 1999. Representing phytoplankton aggregates in biogeochemical models. Deep-Sea Res. I Oceanogr. Res. Pap. 46, 1841–1859 http://dx.doi.org/10.1016/S0967-0637(99)00032-1.
Lam, P., 2011. The dynamic ocean biological pump: insights from a global compilation of particulate organic carbon, CaCO3, and opal concentration profiles from the mesopelagic. Global Biogeochem. Cycles GB3009 http://dx.doi.org/10.1029/2010GB003868.
Lead, J., Wilkinson, K., 2007. Environmental colloids and particles: current knowledge and future developments. In: Wilkinson, K., Leas, J. (Eds.), Environmental Colloids and Particles: Behaviour, Separation and Characterisation, vol. 10. John Wiley & Sons, Ltd, pp. 1–16 (chapter 1).
Lewin, J., 1961. The dissolution of silica from diatom walls. Geochim. Cosmochim. Acta 182–198 http://dx.doi.org/10.1016/S0016-7037(61)80054-9.
Loucaides, S., Behrends, T., van Cappellen, P., 2010. Reactivity of biogenic silica: surface versus bulk charge density. Geochim. Cosmochim. Acta 517–530 http://dx.doi.org/10.1016/j.gca.2009.10.038.
Lozier, M., 2010. Deconstructing the Conveyor Belt. Science 328, 1507 http://dx.doi.org/10.1126/science.1189250.
MacKenzie, F., Stoffyn, M., Wollast, R., 1978. Aluminum in seawater: control by biological activity. Science 199, 680 http://dx.doi.org/10.1126/science.199.4329.680.
Mackin, J., 1986. Control of dissolved al distributions in marine sediments by clay reconstitution reactions: experimental evidence leading to a unified theory. Geochim. Cosmochim. Acta 207–214 http://dx.doi.org/10.1016/0016-7037(86)90170-5.
Mackin, J., Aller, R., 1986. The effects of clay mineral reactions on dissolved al distributions in sediments and waters of the Amazon continental shelf. Cont. Shelf Res. 245–262 http://dx.doi.org/10.1016/0278-4343(86)90063-4.
Madec, G., 2008. NEMO ocean engine. Note du Pole de Modélisation. Institut Pierre-Simon Laplace.
Madec, G., Delecluse, P., Imbard, M., Lévy, C., 1998. OPA 8.1 Ocean General Circulation Model reference manual. Note du Pole de Modélisation, 11. Institut Pierre-Simon Laplace (91p.).
Mahowald, N., Kohfeld, K., Hansson, M., Balkanski, Y., Harrison, S., Prentice, I., Schulz, M., Rodhe, H., 1999. Dust sources and deposition during the last glacial maximum and current climate: a comparison of model results with paleodata from ice cores and marine sediments. J. Geophys. Res. 15895-15 http://dx.doi.org/10.1029/1999JD900084.
Maier-Reimer, E., Mikolajewicz, U., Hasselmann, K., 1993. Mean circulation of the Hamburg LSG OGCM and its sensitivity to the thermohaline surface forcing. J. Phys. Oceanogr. 731–757.
Maring, H., Duce, R., 1987. The impact of atmospheric aerosols on trace metal chemistry in open ocean surface seawater, 1. aluminum. Earth Planet. Sci. Lett. 381–392 http://dx.doi.org/10.1016/0012-821X(87)90003-3.
Martin, J., 1990. Glacial–interglacial CO_2 change: the iron hypothesis. Paleoceanography 1–13.
McAlister, J., Orians, K., 2011. Controls on hydroxide-speciated trace metals in the ocean.
McDonnell, A. et al. (2011). Marine particle dynamics: sinking velocities, size distributions, fluxes, and microbial degradation rates. Ph.D. thesis Massachusetts Institute of Technology.
McDonnell, A., Buesseler, K., 2010. Variability in the average sinking velocity of marine particles. Limnol. Oceanogr. 2085–2096 http://dx.doi.org/10.4319/lo.2010.55.5.2085.
Measures, C., Vink, 2000. On the use of dissolved aluminum in surface waters to estimate dust deposition to the ocean. Global Biogeochem. Cycles 317–327 http://dx.doi.org/10.1029/1999GB001188.
Measures, C., Brown, M., Vink, S., 2005. Dust deposition to the surface waters of the western and central north pacific inferred from surface water dissolved aluminum concentrations. Geochem. Geophys. Geosyst. Q09M03- http://dx.doi.org/10.1029/2005GC000922.
Measures, C., Sato, T., Vink, S., Howell, S., Li, Y., 2010. The fractional solubility of aluminium from mineral aerosols collected in Hawaii and implications for atmospheric deposition of biogeochemically important trace elements. Mar. Chem. 144–153 http://dx.doi.org/10.1016/j.marchem.2009.01.014.
Middag, R. (2010). Dissolved Aluminium and Manganese in the Polar Oceans. Ph.D. thesis University of Groningen.
Middag, R., de Baar, H., Laan, P., Bakker, K., 2009. Dissolved aluminium and the silicon cycle in the Arctic Ocean. Mar. Chem. 176–195 http://dx.doi.org/10.1016/j.marchem.2009.08.002.
Middag, R., van Slooten, C., de Baar, H., Laan, P., 2011. Dissolved aluminium in the southern ocean. Deep-Sea Res. II Top. Stud. Oceanogr. http://dx.doi.org/10.1016/j.dsr2.2011.03.001
Middag, R., de Baar, H., Laan, P., Huhn, O., 2012. The effects of continental margins and water mass circulation on the distribution of dissolved aluminum and manganese in drake passage. J. Geophys. Res. C01019 http://dx.doi.org/10.1029/2011JC007434.
Middag, R., van Aken, H., Hulten, M.M.P., and de Baar, H.J.W. in preparation. Aluminium in the ocean: unique mirror image of the biological cycle.
Moore, J., Braucher, O., et al., 2008. Sedimentary and mineral dust sources of dissolved iron to the world ocean. Biogeosciences 631–656.
Moran, S., Moore, R.M., 1988. Temporal variations in dissolved and particulate aluminum during a spring bloom. Estuarine Coastal Shelf Sci. 27, 205–215 http://dx.doi.org/10.1016/0272-7714(88)90090-X.
Moran, S., Moore, R., 1989. The distribution of colloidal aluminum and organic carbon in coastal and open ocean waters off Nova Scotia. Geochim. Cosmochim. Acta 2519–2527.
Moran, S., Moore, R., 1991. The potential source of dissolved aluminum from resuspended sediments to the north Atlantic deep water. Geochim. Cosmochim. Acta 2745–2751 http://dx.doi.org/10.1016/0016-7037(91)90441-7.
Moran, S., Moore, R., Westerlund, S., 1992. Dissolved aluminum in the Weddell sea. Deep Sea Res. Part A 39, 537–547 http://dx.doi.org/10.1016/0198-0149(92)90087-A.
Obata, H., Alibo, D., Nozaki, Y., 2007. Dissolved aluminum, indium, and cerium in the Sea of Japan and the Sea of Okhotsk: comparison to the marginal seas of the western North Pacific. J. Geophys. Res. C12003- http://dx.doi.org/10.1029/2006JC003944.
Orians, K., Bruland, K., 1985. Dissolved aluminium in the central North Pacific. Nature 316, 427–429 http://dx.doi.org/10.1038/316427a0.
Orians, K., Bruland, K., 1986. The biogeochemistry of aluminum in the Pacific Ocean. Earth Planet. Sci. Lett. 397–410 http://dx.doi.org/10.1016/0012-821X(86)90006-3.
Ragueneau, O., Tréguer, P., Leynaert, A., Anderson, R., Brzezinski, M., DeMaster, D., Dugdale, R., Dymond, J., Fischer, G., Francois, R., et al., 2000. A review of the Si cycle in the modern ocean: recent progress and missing gaps in the application of biogenic opal as a paleoproductivity proxy. Glob. Planet. Chang. 317–365 http://dx.doi.org/10.1016/S0921-8181(00)00052-7.
Rijkenberg, M., Powell, C., Dall'Osto, M., Nielsdottir, M., Patey, M., Hill, P., Baker, A., Jickells, T., Harrison, R., Achterberg, E., 2008. Changes in iron speciation following a Saharan dust event in the tropical North Atlantic Ocean. Mar. Chem. 56–67 http://dx.doi.org/10.1016/j.marchem.2008.02.006.
Rijkenberg, M.J.A., Steigenberger, S., Powell, C.F., van Haren, H., Patey, M.D., Baker, A.R., Achterberg, E.P., 2012. Fluxes and distribution of dissolved iron in the eastern (sub-) tropical North Atlantic Ocean, Global Biogeochem. Cycles 26, GB3004 http://dx.doi.org/10.1029/2011GB004264.
Sarmiento, J., Gruber, N., 2006. Ocean biogeochemical dynamics. Princeton University Press.
Schulz, M., Cozic, A., Szopa, S., 2009. LMDzT-INCA dust forecast model developments and associated validation efforts. IOP Conference Series: Earth and Environmental Science, vol. 7. IOP Publishing, p. 012014.
Slemons, L., Murray, J., Resing, J., Paul, B., Dutrieux, P., 2010. Western Pacific coastal sources of iron, manganese, and aluminum to the Equatorial Undercurrent. Global Biogeochem. Cycles http://dx.doi.org/10.1029/2009GB003693.
Stoffyn, M., 1979. Biological control of dissolved aluminum in seawater: experimental evidence. Science 203, 651 http://dx.doi.org/10.1126/science.203.4381.651.
Stoffyn, M., Mackenzie, F., 1982. Fate of dissolved aluminum in the oceans. Mar. Chem. 105–127 http://dx.doi.org/10.1016/0304-4203(82)90036-6.
Tagliabue, A., Bopp, L., Dutay, J.-C., Bowie, A., Chever, F., Jean-Baptiste, P., Bucciarelli, E., Lannuzel, D., Remenyi, T., Sarthou, G., Aumont, O., Gehlen, M., Jeandel, C., 2010. Hydrothermal contribution to the oceanic dissolved iron inventory. Nat. Geosci. 252–256 http://dx.doi.org/10.1038/NGEO818.
Tagliabue, A., Bopp, L., Gehlen, M., 2011. The response of marine carbon and nutrient cycles to ocean acidification: large uncertainties related to phytoplankton physiological assumptions. Global Biogeochem. Cycles GB3017 http://dx.doi.org/10.1029/2010GB003929.
Textor, C., Schulz, M., Guibert, S., Kinne, S., Balkanski, Y., Bauer, S., Berntsen, T., Berglen, T., Boucher, O., Chin, M., et al., 2006. Analysis and quantification of the diversities of aerosol life cycles within AeroCom. Atmos. Chem. Phys. 1777 http://dx.doi.org/10.5194/acp-6-1777-2006.

Vink, S., Measures, C., 2001. The role of dust deposition in determining surface water distributions of Al and Fe in the South West Atlantic. Deep-Sea Res. II Top. Stud. Oceanogr. 48, 2787–2809 http://dx.doi.org/10.1016/S0967-0645(01)00018-2.
Walker, W., Cronan, C., Patterson, H., 1988. A kinetic study of aluminum adsorption by aluminosilicate clay minerals. Geochim. Cosmochim. Acta 55–62.
Wedepohl, K., 1995. The composition of the continental crust. Geochim. Cosmochim. Acta 1217–1232 http://dx.doi.org/10.1016/0016-7037(95)00038-2.
Whitehead, P., Wilson, E., Butterfield, D., 1998. A semi-distributed Integrated Nitrogen model for multiple source assessment in Catchments (INCA): Part I â€" model structure and process equations. Sci. Total. Environ. -211, 547–558 http://dx.doi.org/10.1016/S0048-9697(98)00037-0.